# Boosting the toolbox for live imaging of translation

Maelle Bellec[1,2], Ruoyu Chen[3,4], Jana Dhayni[5], Antonello Trullo[1], Damien Avinens[6], Hussein Karaki[5], Flavia Mazzarda[5] Helene Lenden-Hasse[1], Cyril Favard[6], Ruth Lehmann[4], Edouard Bertrand[*5], Mounia Lagha[1], Jeremy Dufourt[*1,6]

## Affiliations

[1]Institut de Génétique Moléculaire de Montpellier, Univ Montpellier, CNRS, Montpellier, France.

[2]Department of Developmental Genetics, Max Planck Institute for Heart and Lung Research, Bad Nauheim, Germany.

[3]Vilcek Institute of Graduate Studies, NYU School of Medicine, New York, United States.

[4]Whitehead Institute for Biomedical Research and Department of Biology, Massachusetts Institute of Technology, Cambridge, MA, USA.

[5]Institut de Génétique Humaine, University of Montpellier, CNRS, 34396 Montpellier, France.

[6]Institut de Recherche en Infectiologie de Montpellier, CNRS UMR 9004, University of Montpellier, 1919 Route de Mende, Montpellier, 34293, Cedex 5, France.

* Correspondence to: jeremy.dufourt@irim.cnrs.fr

* Correspondence to: edouard.bertrand@igh.cnrs.fr

**Abstract**

Live imaging of translation based on tag recognition by a single chain antibody is a powerful technique to assess translation regulation in living cells. However, especially in a multicellular organism, this approach is challenging and requires optimization in terms of expression level and detection sensitivity of the system. Here, we improved existing fluorescent tools and developed new ones to image and quantify nascent translation in the living *Drosophila* embryo and in mammalian cells. We tested and characterized five different Green Fluorescent Protein variants fused to the single chain fragment variable (scFv) and uncover photobleaching, aggregation and intensity disparities. Using different strengths of germline and somatic drivers, we determined that the availability of the scFv is critical in order to detect translation throughout development. We introduced a new translation imaging method based on a nanobody/tag system named ALFA-array, allowing the sensitive and simultaneous detection of the translation of several distinct mRNA species. Finally, we developed a largely improved RNA imaging system based on an MCP-tdStaygold fusion.

## Introduction

During development, multipotent cells progressively acquire specific fates leading to the formation of a variety of tissues. This process relies on spatio-temporally regulated gene expression programs, contributing to the reliability and reproducibility of gene expression patterns that generate the final body plan. In this process, the regulation of mRNA translation is a key step since the dynamics of translation in space and time critically affects the outcome of gene expression. Most approaches to study the regulation of translation in whole organisms rely on a bulk population of cells with poor spatial and temporal information. Consequently, the precision and heterogeneity in the regulation of translation at the cellular and molecular level remains incompletely understood. Live imaging methods of translation have been developed in cultured cells[1–5] since 2016 and recently introduced in *Drosophila*[6–8]. These methods are based on the fluorescent labeling of nascent peptide chains. The labeling system is made of two components, a genetically-encoded antibody such as a single-chain variable fragment antibody (scFv) or Fab fragment[9–11] fused to a fluorescent protein (FP; referred to as the detector), and a N-terminal peptide epitope inserted in multiple copies in frame with the gene of interest[12]. These live imaging approaches made it possible to visualize translation up to the single-molecule scale in cultured cells but also in an entire organism[7,8]. Such technological breakthroughs provided important insights in our understanding of gene regulation through translation and, for instance, revealed the existence of motor-driven polysome transport and spatial heterogeneity of translation at the subcellular level[1,4,7,13–17].

The discovery of the *Aequorea victoria* green-fluorescent protein[18,19] and especially its optimized version mEGFP[20] have revolutionized imaging of biological processes[21]. Since then, several new FPs have been and continue to be discovered and

61 engineered[22,23]. The constant race for better FPs generally implies the optimization for
62 fast folding, pH resistance as well as improvement of photo-physic properties[24].
63 Introduction of the bacteriophage-derived MS2 RNA binding sites, which are
64 recognized by MS2 Coat Protein (MCP) fused to FP, provided a technique to visualize
65 transcription in living cell. This technological advance has been subjected to several
66 improvements from its initial development in 1998[25]. These improvements include
67 increased sensitivity down to single molecules[26], implementation in a living organism[27],
68 the generation of new stem loops to visualize single mRNAs at a high temporal
69 resolution[7,28], artefact-free RNA tags[29] and double mRNA species imaging with an
70 orthologous system[30]. However, several limitations exist with the present tools that
71 hinder quantitative imaging. For example, protein aggregation has been observed for
72 some systems derived from MS2 Coat Protein fused to GFP[29,31,32] and for scFv fused
73 to specific GFP variants[12]. Furthermore, the expression level of the detector is critical
74 to ensure accurate detection, particularly for translation, as most of the time one mRNA
75 undergoes multiple rounds of translation. However, no such optimization has been
76 made for the SunTag system in the context of a developing organism, although photo-
77 physical properties of molecules can be variable between different systems (i.e. *in vitro*
78 experiments, cell culture, tissues, organisms…)[24,33,34].
79 Here, we tested different GFP variants for their brightness, photobleaching and
80 propensity to aggregation in fixed and live *Drosophila* embryos. We also generated
81 inducible scFv-FP constructs that, when combined with different drivers, extend the
82 use of the SunTag system to a wider range of genes and biological questions.
83 Furthermore, we developed an orthologous method, called ALFA-array, to visualize
84 nascent translation in *Drosophila* embryo and mammalian cells. This system is based

85 on a small and soluble nanobody and we show its usefulness by combining it with the
86 SunTag to visualize translation of two different mRNA species in *Drosophila* embryos.
87

88 **Results**

89 **New fluorescent protein fused to scFv to detect nascent translation.**

90 The SunTag method is a bipartite system based on an antibody-derived single chain
91 variable fragment (scFv) detector, fused to the GB1 solubility tag and to a fluorescent
92 protein (FP; the detector). The scFv binds a peptide named Supernova Tag (suntag)
93 derived from the yeast GCN4 protein and genetically fused in multiple copies at the N-
94 terminus of the gene of interest[35] (Figure 1a). To improve the system, we created new
95 scFvs with different green fluorescent proteins under the control of *nanos* (*nos*)
96 enhancer-promoter (EPr). This EPr combination drives expression in the *Drosophila*
97 germline[36–39] allowing the maternal deposition of mature scFv-FP into laid eggs (Figure
98 S1A). We generated a set of four different constructs, in addition to the previously
99 published scFv fused to the superfolder GFP (sfGFP)[40] in *Drosophila*, named scFv-
100 sfGFP[7]. The new generation of green fluorescent protein variants includes: i) the
101 monomeric superfolder GFP2 (msGFP2)[41], ii) the mGreenLantern (GL)[42], iii)
102 mNeonGreen (NG)[43] and iv) the monomeric *A. victoria* fluorescent protein 1 (mAvic1)[22]
103 (Figure 1b, upper panel). Live imaging of these five scFv-FPs during embryonic
104 development until the end of nuclear cycle 14 (n.c. 14) showed that all the scFv-FPs
105 are well expressed, localize mainly in the nucleus due to the presence of a nuclear
106 localization signal, and do not form aggregates (Figure S1b and movie Sup 1-5).
107 Quantification of the fluorescent intensity during the first forty minutes of n.c.14,
108 showed that the apparent brightness of these four new scFv was similar to the scFv-
109 sfGFP, while scFv-mAvic1 produced brighter signals (Figure S1c) and scFv-GL was

110 prone to photobleaching (Figure S1c). We confirmed that the distribution of scFv-FP
111 was homogenous in the embryo and dots/aggregates were not detected by light-sheet
112 imaging of the two brightest scFv-FPs, scFv-mAvic1 and scFv-msGFP2 (Figure S1d
113 and movie Sup 6-7).
114 We next tested the capacity of these new scFv-FPs to detect mRNA in translation in
115 *Drosophila* embryos. We crossed the different scFv-FP lines into the background of a
116 *twist* gene endogenously tagged with MS2 and suntag (*twi_suntag_MS2_CRISPR*)
117 (Figure 1b, lower panel) and performed single-molecule Fluorescent *in situ*
118 Hybridization (smFISH) on fixed embryos to detect the tagged mRNAs. Actively
119 translated mRNAs (polysomes) were then visualized as co-localized GFP and mRNA
120 spots. Imaging the border of *twist* mRNA transcription pattern showed that the
121 translation signal was present only in the described pattern of *twist* expression
122 (mesoderm)[44] (Figure 1c), supporting that the signal is specific. For all scFv-FPs, we
123 observed a clear colocalization between mRNA (red signal) and polysomes (green
124 signal) in addition to mRNA molecules that were not detectably translated (Figure S1e).
125 Notably, a fainter signal was detected in fixed samples for polysomes labeled with
126 scFv-mAvic1 at this stage of embryogenesis, as compared to its high apparent
127 brightness in live samples (Figure S1f), suggesting that mAvic1 is more sensitive to
128 the fixation/smFISH protocol. Immuno-smFISH with an antibody against GFP did not
129 improve the signal but increased the background. Surprisingly, we found that staining
130 with only a secondary antibody could label nascent foci of translation (Figure S2a), and
131 only when the scFv-FP was present (Figure S2b). This result suggested that secondary
132 antibodies alone could bind scFv-FP. Experiments using immunofluorescence and
133 scFv-FP simultaneously should thus be avoided. We then looked at the behavior of
134 these scFv-FPs in live embryos in the presence of *twi_suntag_MS2_CRISPR*. We

135 could observe bright green fluorescent dots in movement within the mesoderm (Figure
136 1d, movie sup 8-12). To characterize the detection capacity of each FP in live embryos,
137 we measured the mean intensity of all detected spots for 4 min during n.c. 14 with a
138 high temporal resolution (Figure 1e, movie sup 8-12). The translation foci detected by
139 scFv-mAvic1, scFv-sfGFP and scFv-msGFP2 showed a stable signal compared to
140 scFv-NG and scFv-GL (Figure 1e). Collectively, these results show that the four new
141 scFv-FPs are able to bind nascent suntag peptides and can therefore detect mRNA
142 being translated in live and fixed samples.
143
144 **New scFv-FP prevents aggregate formation**
145 To show whether scFv-FPs expressed under the maternal *nos* EPr could detect
146 translation during late embryogenesis, we imaged fixed embryos at the gastrulation
147 stage. We observed that the tagged Twist protein localized to nuclei in the ventral
148 gastrulation furrow region, consistent with Twist being a mesodermal transcription
149 factor (Figure S2c, upper panel). To test, whether the presence of a NLS in the scFv-
150 FP construct might be responsible for this nuclear localization, we imaged the
151 localization of the Insulin-like peptide 4 (Ilp4), an excreted protein expressed in the
152 mesoderm[45]. We used the tagged Ilp4 with suntag and observed scFv containing the
153 NLS in the cytoplasm (Figure S2c, lower panel). Thus, at least in these cases, the
154 presence of a NLS in the scFv-FP construct appears not to significantly interfere with
155 the native localization of tagged proteins.
156 Strikingly, at the gastrulation stage, bright GFP spots were observed only when using
157 scFv-sfGFP in *twi_suntag_MS2_CRISPR* embryos but not with the other scFv-FPs
158 (Figure S3a). As only the FP sequences are different between these constructs, this
159 discrepancy might be due to a difference in protein stability, i.e. scFv-sfGFP being

160 more stable than the other variants, or being more prone to aggregation. To distinguish
161 between these possibilities, we used smFISH to label *twi_suntag_MS2_CRISPR*
162 mRNA in the presence of the different scFv-FPs to determine whether the bright GFP
163 spots observed during gastrulation co-localized with mRNA and represent true
164 translation spots. With scFv-sfGFP we saw large green spots that were not co-localized
165 with mRNA (Figure S3b upper left panels, white arrowhead). We did not observe these
166 large spots with any of the four new scFv-FPs (Figure S3b) suggesting an aggregation
167 of the scFv-sfGFP in the *Drosophila* embryo at the gastrulation stage in the presence
168 of *twi_suntag_MS2_CRISPR*.
169 We next asked whether aggregation was specific for the tagged *twi* in developing
170 embryos or could also occur in cultured cells. We expressed scFv-sfGFP and scFv-
171 msGFP2 in *Drosophila* S2R+ cells along with a SunTag-luciferase reporter
172 (SunTagRLuc-MS2; see methods and Figure S3c). The SunTagRLuc-MS2 plasmid
173 was co-transfected with an scFv-FP plasmid as well as an MCP-Halotag plasmid to
174 track single mRNA molecules and their translation during live-cell imaging. As
175 expected, scFv-FPs were able to label polysomes by forming GFP foci that co-localized
176 with mRNAs (Figure S3d). With the scFv-sfGFP, however, we frequently observed
177 GFP aggregates which were not associated with any mRNA molecules. These
178 aggregates were morphologically distinct from translating foci and were more abundant
179 and bigger than the GFP aggregates observed in gastrulating embryos (Figure S3d-
180 e). This result suggests an aggregation of the SunTag peptides bound by the scFv-
181 sfGFP after being translated and released from polysomes. Although few aggregates
182 were also present in cells expressing scFv-msGFP2 with the SunTagRLuc-MS2
183 reporter (Figure S3d), this occurred with a significantly lower frequency (~55% of cells

184 without aggregates compared to ~15% using scFv-sfGFP) and smaller aggregate size,
185 suggesting that msGFP2 is less prone to aggregate formation.
186 These results support that the scFv-FPs containing newer generation monomeric FPs
187 are more suitable for translation analysis, as they are less likely to form aggregates
188 compared to sfGFP which is able to form weak dimers[41,46].
189

190 **Monitoring translational arrest during *Drosophila* embryogenesis**

191 The low amount of translation spots observed during gastrulation with scFv-sfGFP
192 suggested that *twi* translation maybe have ceased at this stage of development (Figure
193 S3a-b). However, a translational arrest of *twist* mRNAs has not been described
194 previously. This unexpected observation led us to verify whether *twi* transcripts were
195 undergoing a translational arrest during n.c.14 (Figure 2a), and for this we used the
196 four new scFv-FPs. Interestingly, we found that at mid-late n.c. 14 (Figure 2a), the
197 *twi_suntag_MS2_CRISPR* RNA was mostly translated at the border of the mesoderm
198 (Figure 2b and S4a-c). Using scFv-msGFP2 fluorescence intensity quantification, the
199 percentage of mRNA in translation was slightly lower in the center as compared to the
200 border of the mesoderm (44 ± 4% at the center and 61 ±1% at the border see methods).
201 Strikingly, the polysomes intensities were much lower in the center compared to the
202 mesoderm border, suggesting reduced translation (Figure 2b and S4a-c). A
203 translational arrest was recently described for *Hunchback* (*Hb*) using the SunTag
204 system in the *Drosophila* embryo[8]. In this study the authors showed that after being
205 translated in the entire Hb domain (anterior half of the embryo), *hb* translation became
206 restricted to the border of its expression pattern, similarly to what we observed for *twist*.
207 At least two models can explain this result: i) *twi* translation is actively repressed at first
208 in regions where the RNA and protein expression is highest (as suggested for *hb*[8]), or

209 ii) the amount of scFv-FP becomes limiting during mid-late n.c. 14 at first in regions
210 where the RNA and protein expression is highest and prevents the detection of
211 translation (Figure 2c upper panel). To test these hypotheses, we used the
212 *twi_suntag_transgene*, which exhibits a stochastic expression pattern, belated
213 transcriptional activation[7] and thus lower mRNA level as compared to
214 *twi_suntag_MS2_CRISPR.* If *twi* translation is actively repressed, a similar
215 translational arrest should be observed for the *twi_suntag_transgene*. In contrast, if the
216 amount of scFv-FP is limiting, translation of the transgene should be detectable over a
217 longer period of time (Figure 2c). Using live imaging, we observed translation spots of
218 the *twi-suntag_transgene* at a stage when *twi_suntag_MS2_CRISPR* translation spots
219 vanished (Figure 2d, S4d and Movie S13-15). The translation dots of the
220 *twi_suntag_transgene* colocalized with mRNA dots in late n.c. 14 and gastrulation
221 stage as confirmed with smFISH (Figure S4e). These results suggest that the amount
222 of scFv-FP might be limiting when *twi* translation is monitored from its endogenous
223 locus (*twi_suntag_MS2_CRISPR* allele), preventing detection of translation at
224 gastrulation.
225 To confirm this hypothesis, we used an antibody against the suntag peptides (anti-
226 GCN4) in the absence of scFv-FP and saw translation of *twi_suntag_MS2_CRISPR*
227 mRNAs even at mid-late n.c. 14 and gastrulation stage (Figure 2e and S5a). Moreover,
228 the percentage of mRNA in translation was homogenous within the mesoderm (72 ±4%
229 at the border and 68 ±2% at the center) and polysome intensity between center and
230 border was similar (Figure 2e), in contrast to the results obtained with scFv-msGFP2
231 (Figure 2b). Altogether these results demonstrate that there is no translational arrest
232 of *twi* mRNAs during n.c.14. Instead, the amount of scFv-FP expressed under the
233 maternally active *nos* EPr becomes insufficient to detect translation during gastrulation,

234 when a large pool of tagged mRNAs is translated. Our experiments suggest that anti-
235 GCN4 antibodies should be used as a control to distinguish between true endogenous
236 repression of translation and mere experimentally-dependent depletion of the labelling
237 reagent.
238
239 **Inducible scFv-FP allows imaging of translation during embryogenesis**
240 To overcome the limited amount of scFv-FP and allow the sustained imaging of *twi*
241 translation from egg laying to gastrulation, we used the UAS/Gal4 system to increase
242 the expression of scFv-FP during oogenesis. We generated four lines with the different
243 *scFv-FPs* downstream of a *UASp* promoter (Figure 3a and S6a) and crossed these
244 with the maternal *nos-Gal4* driver (Figure 3b). No aggregation was detected in live
245 embryos (Figure S6a, Movie S16-19 and see methods). To quantify the amount of free
246 scFv-FP using *nosEPr-scFvmsGFP2* or *nos-Gal4>UASp-scFv-msGFP2,* we
247 performed Fluorescence Correlation Spectroscopy (FCS) at early/mid n.c.14 in the
248 mesoderm of embryos. Fluorescence signal corresponding to free scFv-msGFP2 was
249 recorded and fitted with diffusion models (Figure S6b). On average, ~28 times more
250 free scFv-msGFP2 molecules were available in the confocal volume using *nos-*
251 *Gal4>UASp-scFv-msGFP2* compared to *nosEPr-scFvmsGFP2* at early/mid n.c.14 (
252 ~710 and ~25 free scFv-msGFP2 respectively) (Figure S6c). Using this system , we
253 asked if it would allow detection of *twi* translation until late n.c. 14 and gastrulation
254 stage. In *twi_suntag_MS2_CRISPR* embryos with maternally provided *nos-*
255 *Gal4>UASp-scFv-msGFP2* we saw that *twi* mRNAs were translated throughout n.c.14
256 (Figure 3c), even in the most ventral part of the embryo, at the center of the *twi* domain
257 of expression (Figure 3c). However, we were not able to detect small dots of scFv-FP,
258 most likely corresponding to individual mature proteins, probably due to the lower

259 signal-to-noise ratio generated by the increased levels of free *scFv-msGFP2*. We also
260 observed translation dots at the gastrulation stage in fixed *twi_suntag_MS2_CRISPR*
261 embryos with *nos-Gal4>UASp-scFv-msGFP2* (Figure 3d left panels) but not with *EPr-*
262 *scFv-msGFP2* (Figure 3d right panels). Similar results were observed with live
263 imaging, where *twi_suntag_MS2_CRISPR* mRNAs were translated until gastrulation
264 with *nos-Gal4>UASp-scFv-msGFP2* (Figure 3e and Movie S20) but not with *EPr-scFv-*
265 *msGFP2.* Control embryos lacking *twi_suntag_MS2_CRISPR* mRNAs did not show
266 any translation spot at any stage (Figure 3e and Movie S20). These results indicate
267 that the use of *nos-Gal4>UASp-scFv-msGFP2* would be more suitable to detect
268 translation until gastrulation. The *UASp* promoter drives expression in the germline but
269 is less efficient in somatic tissues[47]. On the contrary, the *UASt* containing *HSP70*
270 promoter drives expression in the somatic tissue[48]. Recently, the *UASt* promoter has
271 been modified to obtain a promoter, called *UASz*, to drive expression in both somatic
272 and germline tissues and being expressed at least four times higher than *UASp*[49]. Due
273 to the high amount of free scFv observed with the *UASp-FP* lines, we generated a new
274 promoter derived from the *UASz*, in which we removed the translational enhancer *IVS-*
275 *Syn21*[49] to prevent excessive expression of free scFv-FP and obtain a better signal-
276 to-noise ratio (Figure S7a, b). This new promoter named *UASy* was fused to the *scFv-*
277 *msGFP2* and crossed with the *nos-Gal4* driver line. As all the other constructs
278 generated in this study, *nos-Gal4>UASy-scFv-msGFP2* alone did not lead to
279 aggregates during early embryogenesis (Figure S7b and Movie S21). Unfortunately,
280 the translation of *twi_suntag_MS2_CRISPR* mRNA at the end of n.c. 14 showed a
281 similar pattern – although less pronounced – as with *scFv-msGFP2* where translation
282 was mostly present at the border of *twi* pattern (Figure S7c), likely due to the weaker
283 expression of the *UASy* compared to *UASp* promoters and subsequent depletion of

284 scFv in the central mesoderm. Maternal expression of the scFv-FP constructs limits
285 our ability to observe translational dynamics at later stages in development. To
286 overcome this, we crossed *UASy-scFv-msGFP2* with an early zygotic *nullo-Gal4* driver
287 to express throughout the embryo. We observed scFv-msGFP2 expression at the
288 beginning of gastrulation (Movie S22) and a strong and homogeneous expression in
289 somatic tissues of later embryos (Figure S7d). We conclude that the *nos-Gal4>UASp-*
290 *scFv-FP* represents a good tool to image translation from early embryogenesis to
291 gastrulation stage and that the new *UASy-scFv-msGFP2* would enable the imaging of
292 translation in somatic cells at later stages.
293
294 **Development of the ALFA-array system to monitor translation in *Drosophila***
295 After having optimized the scFv-FP-based detector, we sought to generate an
296 optimized orthologous system to the SunTag to detect the translation of two different
297 mRNA species in *Drosophila*. To this end, we searched for a highly specific
298 nanobody/tag pair and decided to use the recently developed ALFA-Tag[50]. The ALFA-
299 Tag is a small peptide that harbors several advantages: its synthetic sequence is
300 absent from the proteome of model organisms, its sequence is smaller than that of the
301 SunTag sequence (15 amino acid compared to 19, respectively Figure 4a), it is
302 monovalent, hydrophilic and was effective in *Drosophila* for protein manipulation[51].
303 Finally, the nanobody anti-ALFA detector (NB-ALFA) is smaller than the scFv (Figure
304 4b), is quite soluble and displays a very strong affinity for the ALFA-Tag (measured at
305 26 pM)[50]. Taking advantage of these properties, we multimerized the ALFA-Tag
306 sequences to create a 12x and 32x_ALFA-array. Each ALFA-tag sequence was
307 flanked by a proline to reduce potential influence of neighboring secondary structures,
308 and a spacer of 5 amino acid (GSGSG) to minimize steric hindrance of neighboring

309 peptide binding sites (Figure 4a, c). The NB-ALFA was fused to the msGFP2 and to
310 the GB1 solubilization tag (also used for the scFv) to avoid potential aggregation
311 caused by the multimerization of ALFA-tag sequences. Finally, we generated a
312 *Drosophila* line with the *NB-ALFA-msGFP2* under the control of *nos* EPr (*NB-ALFA-*
313 *msGFP2)*. The system was also tested in mammalian cells (see below).
314 To study translation in *Drosophila* embryos using the 32x_ALFA-array system, we
315 chose to tag the *Ilp4* gene, which codes for a small protein. We reasoned that if we
316 could visualize the translation of a very short transcript/protein, the tool would work
317 even better for longer ones. A 32x_ALFA-array was inserted between the *Ilp4* initiation
318 codon and *Ilp4* gene body, appended with *Ilp4* UTRs and *Ilp4* EPr (*Ilp4_32x_ALFA-*
319 *array*, Figure 4d). In absence of fluorescent detector expression, we found by smFISH
320 that the *Ilp4_32x_ALFA-array* was expressed in the mesoderm of early *Drosophila*
321 embryos (Figure S8a), consistent with previous reports for *Ilp4*[45]. Moreover,
322 immunofluorescence with the anti-ALFA antibody showed bright dots specifically
323 colocalizing with *Ilp4_32x_ALFA-array* mRNAs and thus representing foci of
324 translation (Figure S8b-c). Importantly, the *Ilp4_32x_ALFA-array* was not recognized
325 by the anti-GCN4 antibody (Figure S8a).
326 We next confirmed by live imaging that the *NB-ALFA-msGFP2* strain was expressed
327 during embryonic development until the end of n.c.14, that it was mainly localized to
328 the nucleus and that it did not form any aggregates or foci in absence of tagged mRNA
329 (Figure S8d and Movie S23). Then, the *Ilp4_32x_ALFA-array* was crossed with *NB-*
330 *ALFA*-msGFP2. The resulting embryos showed bright GFP spots overlapping with
331 *Ilp4_32x_ALFA-array* mRNAs (Figure 4d), showing the ability of NB-ALFA-msGFP2 to
332 bind the nascent 32x_ALFA-array *in vivo.* Next, we monitored translation in live
333 embryos and observed bright GFP dots appearing on the ventral side of the embryo

334 (Figure 4e and Movie S24). The signal was restricted to the mesoderm during n.c.14
335 (Figure S8e and Movie S25) and became more restricted to the ventral furrow during
336 gastrulation (Figure S8f and Movie S25), demonstrating the specificity of the signals.
337 Thus, the *Ilp4_32x_ALFA-array* – NB-ALFA-msGFP2 system is a useful alternative
338 tool to detect mRNA translation during early embryogenesis.
339 Additionally, staining with a secondary antibody alone could label the translation foci
340 only when the NB-ALFA-msGFP2 is present (Figure S9a-b). This was also observed
341 with the scFv-FPs (see above Figure S2a-b), suggesting that secondary antibodies
342 can directly bind both the NB-ALFA-msGFP2 and the scFv-FP (Figure S2a-b and
343 Figure S9a-b). Knowing that the only common part between NB-ALFA and scFv is the
344 GB1 solubility domain, we tested whether this domain was responsible for binding
345 secondary antibodies. We removed the GB1 from the scFv-msGFP2 and NB-ALFA-
346 msGFP2, expressed them in *Drosophila* S2R+ cells and performed Western-blot
347 analyses (Figure S9c). All the scFv and NB-ALFA constructs (with and without the
348 presence of the GB1) could be detected by an anti-GFP antibody in combination with
349 a suitable secondary antibody. However, when using secondary antibodies alone, the
350 constructs with GB1 were still detected, while no band was observed with the
351 constructs without GB1 (Figure S9c). These results demonstrate the direct binding of
352 the GB1 solubilization domain by secondary antibodies.
353 To test if we could use the ALFA-array system in combination with the SunTag to image
354 the translation of two distinct mRNA species in the same embryo, the *Ilp4_32x_ALFA-*
355 *array* was crossed with the *twi_suntag_transgene* (Figure 4f). Using immuno-smFISH
356 in n.c.14 embryos, we observed the two correct expression patterns of Twi and Ilp4,
357 including in the posterior region where only Twi is present (Figure S10a). With higher
358 resolution images, we could visualize single molecules of *Ilp4* mRNA in translation well

359 distinct from *twi* mRNA translation dots (Figure 4g). Furthermore, we were able to
360 distinguish the localization of the Ilp4 protein in the cytoplasm from the Twi protein in
361 the nucleus (Figure 4h). Finally, we then combined four different transgenes, to
362 express scFv-mScarlet, NB-ALFA-msGFP2, *Ilp4_32x_ALFA-array* and
363 *twi_suntag_MS2_CRISPR* in the same embryo. We were able to live image
364 simultaneously the translation of *Ilp4* and *twi* mRNAs (Figure 4i, S10b and Movie S26)
365 in live embryos. Furthermore, we were again able to clearly distinguish the localization
366 of Ilp4 protein in the cytoplasm from Twi protein in the nucleus of live embryos (Figure
367 4j, S10c and Movie S27). Together, these results demonstrate that the 32x_ALFA-
368 array can be used in conjunction with the SunTag system to study the translation of
369 two different mRNAs during *Drosophila* early embryogenesis in live and fixed samples.
370

371 **Development of the ALFA-array system to monitor translation in human cells**

372 To test the performance of the ALFA-tag labeling system to image translation in a
373 different model, we turned to mammalian cells. We first generated HeLa cells
374 expressing a NB-ALFA-sfGFP recombinant nanobody. To evaluate the binding
375 properties of the nanobody for the ALFA tag *in vivo* (measured at 26 pM in vitro[50]) we
376 took advantage of the available H2B_mCherry_ALFAtag constructs[51]. We performed
377 Fluorescence Recovery After Photobleaching (FRAP) of the NB-ALFA-sfGFP, knowing
378 that H2B itself has a very slow recovery time lasting hours[52]. This experiment showed
379 little recovery of NB-ALFA-sfGFP in 5 minutes (Figure S11 a and b), indicating that it
380 is stably bound to its target *in vivo*.

381 Next, we evaluated the performance of the ALFA-array system to image translation in
382 HeLa cells. We inserted a 12x_ALFA-array repetition at the N-terminus of the
383 DYNC1H1 gene by CRISPR-mediated knock-in (Figure 5a), as previously done for the

384 SunTag[4]. Heterozygous clones were obtained and imaged with and without a thirty-
385 minute puromycin treatment to inhibit translation. In untreated cells, bright foci were
386 observed in the cytoplasm, which disappeared following puromycin addition (Figure
387 5b). In addition, smiFISH against the endogenous DYNC1H1 mRNAs revealed that the
388 bright ALFA-tag foci colocalized with single mRNAs (Figure 5c), confirming that these
389 corresponded to DYNC1H1 polysomes. The quality of the signals obtained with only
390 12 repeats of the ALFA-tag demonstrates the efficiency of this labeling system to image
391 translation.
392 Finally, an optimal system to visualize RNA is very useful to image translation at the
393 level of single molecules[1–5]. While the MS2/MCP system provides a very nice way to
394 image single RNAs, it is still limited by the low brightness of the signals and its rapid
395 photobleaching. To improve RNA imaging, we took advantage of the recently
396 developed Staygold fluorescent protein, which is bright and exceptionally
397 photostable[53]. Staygold is an obligate dimeric fluorescent protein, and we thus made
398 a tandem dimer version (tdStaygold) by degenerating its sequence and separating two
399 monomers with a (SAGG)x5 linker. This dimeric version of Staygold was then fused to
400 MCP and used to image RNA in a previously developed HeLa cell line expressing an
401 HIV-1 reporter RNAs tagged with 128 MS2 sites[54]. In this system, the MS2 tag is
402 intronic and enables to label nascent RNAs as well nucleoplasmic pre-mRNAs. Live
403 cells were imaged using a frame rate of one 3D image stack every ten seconds for up
404 to 6 hours (Figure 5d). Single RNAs were observed with both NLS-MCP-tdStaygold
405 and the previously used NLS-MCP-eGFP[54]. However, the signal bleached rapidly with
406 NLS-MCP-eGFP, and single RNAs were no longer detectable after 120 minutes. In
407 contrast, the signal showed little photobleaching with NLS-MCP-tdStaygold and single
408 RNAs were efficiently detected through all the movie, and kept their initial brightness

409 (Figure 5e-f). The NLS-MCP-tdStaygold developed here thus shows largely improved
410 performance for RNA imaging.
411
412 **Discussion**
413 Amplification of biological signals is crucial to study many biological processes with a
414 high spatio-temporal resolution and single-mRNA-molecule sensitivity. Live imaging of
415 translation at single molecule resolution is a relatively recent technology implemented
416 in 2016 in tissue culture and in 2021 in multicellular organisms. In this study, we provide
417 an expanded toolbox to image translation in living cells and organisms. We will discuss
418 some of the limitations and challenges that need to be considered to obtain robust and
419 reliable results.
420 Our data show that the choice of the fluorescent protein is a key element for the signal
421 quality of translation imaging-based systems. The development of fluorescent proteins
422 is a very rapidly evolving field and FP-based tools need to be updated to optimize their
423 use. Often, the choice of the FP needs to be empirically defined for each cell type,
424 tissue or organism studied[55–60]. One important aspect in this choice is the monomeric
425 property of the FP to prevent aggregation issues. Although the sfGFP (a weak dimer)
426 was the standard FP for fusion with the scFv in mammalian cell culture, we found that
427 it might present aggregation issue in *Drosophila.* Local translation of specific mRNAs
428 is an important biological process to control gene expression in space and time. To
429 obtain quantitative answers it is necessary to precisely resolve the location of mRNAs
430 and where their translation occurs. In the present experimental designs, with the
431 orthologous scFv and the NB-ALFA, the use of secondary antibodies can confound
432 signal interpretation as they appear to bind the scFv and NB-ALFA fusion. We
433 demonstrate that this binding is due to the GB1 solubilization domain added to limit

434 aggregation and is in line with a recent study in plants, which showed a strong affinity
435 between GB1 and IgG[61]. As the GB1 is required to for the solubility of the detector,
436 combining translation imaging with immunofluorescence must be carried out with great
437 care, and could require a trial with fluorescent primary antibodies.
438 An important aspect in imaging live embryos or tissues is signal amplification to
439 increase the signal-to-noise ratio. Indeed, in systems like the MS2/MCP, llama-
440 Tag/Fluorescent protein[62] or scFv/SunTag and their derivatives, the signal appears by
441 local specific accumulation of fluorescent detector, over a diffuse background of
442 molecules freely diffusing in the cells. To improve the signal-to-noise ratio,
443 development of Quenchbody (Q-body) could in theory allow background free detection
444 of translation as well as single mRNA[63]. Currently, the signal-to-noise ratio is optimized
445 by reducing the amount of free fluorescent detector and therefore the background. This
446 is achieved by using weak promoters or targeting the free fluorescent detector to other
447 cellular compartments such as the nucleus, or specific organelles for cytoplasmic
448 analysis. However, one should be careful that the availability of these fluorescent
449 detector does not become limiting as more and more RNAs and proteins are produced
450 during development. As we illustrate here, the available concentration of the detector
451 can be a major challenge in developing organisms, especially when the source of the
452 detector is controlled by an endogenous promoter and when the amount of template
453 mRNA in translation is important. This limitation can also be particularly important when
454 a burst of translation occurs such as during viral infection[14,64]. We provide a direct
455 example for detector limitation during early embryogenesis. Here, early activated
456 genes such as *twist* are highly and rapidly transcribed and translated leading to rapid
457 depletion of free detector. We demonstrate the importance of distinguishing between
458 detector depletion and cessation of translation by validating the results with direct

459 immunostaining. We also show that increasing the expression of the detector can
460 overcome the detection problem, however, it will reduce the signal-to-noise ratio and
461 has thus to be taken into consideration for the specific experimental design. In order to
462 reach conditions that can most accurately capture the dynamics of translation, diverse
463 *UAS* promoters together with a variety of available Gal4 drivers should be tested
464 depending on the tissue of interest and the expression level of the tagged gene.
465 Studies on mRNA localization and local translation have speculated that different
466 mRNAs species may be translationally co-regulated[65–67]. To obtain independent
467 translational readouts of different mRNA simultaneously, one can combine orthogonal
468 tagging systems such as hybrid scFvs such as HA or FLAG frankenbody[68–70] or
469 MoonTag nanobodies[16]. In Boersma et al., the authors inserted the MoonTag and the
470 SunTag[16] into different translational reading frames of the same RNA. This allowed to
471 observe in real time heterogeneities in the start site selection of individual ribosomes
472 on a single mRNA molecule. Here, we introduce a new antibody-based detector/tag
473 pair to image translation in living cells and organisms based on multimerization of the
474 ALFA-Tag. The ALFA-array system has a number of advantages: i) it comes from
475 synthetic design and its sequence is thus absent from organisms; ii) the tag is small,
476 soluble, hydrophilic and lacks aldehydes-sensitive amino acids altered by fixation; iii)
477 the detection is through a nanobody, which is small and soluble, has a very high affinity
478 for the ALFA-Tag ($K_d$ of 27 pM), favorably comparable to the MoonTag (Kd of 30 nM)[16].
479 The new translation imaging system described in this study should be applicable to
480 many different organisms to visualize protein localization and control of translation.
481 Moreover, the availability of several orthogonal systems will allow to better analyze of
482 the complexity of translation dynamics by simultaneously comparing several mRNA in
483 diverse cellular environments and conditions. The wide range of applications of the

484 ALFA-array system, coupled with other antibody-based translation detector, provides
485 to the scientific community a highly versatile toolbox to study translation at the single
486 molecule level in cell lines and multicellular organisms. The combination of nascent
487 protein visualization with improved RNA imaging such as the one provided by the NLS-
488 MCP-tdStaygold will facilitate future scientific breakthroughs.
489

490 **Online methods**

491 **Reagents created in this study**

| Reagent type | Genotype | Insertion type and chromosome number | Additional information |
|---|---|---|---|
| *Drosophila* line | *nosEPr > scFv-msGFP2* | Landing site insertion vk33 – Chr. III | mini-white marker, plasmid also available (in pBPhi vector) |
| *Drosophila* line | *nosEPr > scFv-GL* | Landing site insertion vk33 – Chr. III | mini-white marker, plasmid also available (in pBPhi vector) |
| *Drosophila* line | *nosEPr > scFv-mNeonGreen* | Landing site insertion vk33 – Chr. III | mini-white marker, plasmid also available (in pBPhi vector) |
| *Drosophila* line | *nosEPr > scFv-mAvic1* | Landing site insertion vk33 – Chr. III | mini-white marker, plasmid also available (in pBPhi vector) |
| *Drosophila* line | *nosEPr > scFv-msGFP2* | Landing site insertion vk27 – Chr. II | mini-white marker, plasmid also available (in pBPhi vector) |
| *Drosophila* line | *nosEPr > scFv-GL* | Landing site insertion vk27 – Chr. II | mini-white marker, plasmid also available (in pBPhi vector) |
| *Drosophila* line | *nosEPr > scFv-mNeonGreen* | Landing site insertion vk27 – Chr. II | mini-white marker, plasmid also available (in pBPhi vector) |
| *Drosophila* line | *nosEPr > scFv-mAvic1* | Landing site insertion vk27 – Chr. II | mini-white marker, plasmid also available (in pBPhi vector) |
| *Drosophila* line | *UASp > scFv-msGFP2* | Landing site insertion vk33 – Chr. III | mini-white marker, plasmid |

| | | | |
|---|---|---|---|
| | | | also available (in pBPhi vector) |
| *Drosophila* line | *UASp > scFv-GL* | Landing site insertion vk33 – Chr. III | mini-white marker, plasmid also available (in pBPhi vector) |
| *Drosophila* line | *UASp > scFv-mNeonGreen* | Landing site insertion vk33 – Chr. III | mini-white marker, plasmid also available (in pBPhi vector) |
| *Drosophila* line | *UASp > scFv-mAvic1* | Landing site insertion vk33 – Chr. III | mini-white marker, plasmid also available (in pBPhi vector) |
| *Drosophila* line | *UASy > scFv-msGFP2* | Landing site insertion - vk33 Chr. III | mini-white marker, plasmid also available (in pBPhi vector) |
| *Drosophila* line | *nosEPr > NB-ALFA-msGFP2* | Landing site insertion - vk33 Chr. III | mini-white marker, plasmid also available (in pBPhi vector) |
| *Drosophila* line | *Ilp4_32x_ALFA-array* | Landing site insertion - vk33 Chr. III | mini-white marker, plasmid also available (in pBPhi vector) |
| DNA plasmid | NB-ALFA in pUC57-Simple | N/A | Synthetized by Genescript, codon optimized |
| DNA plasmid | ALFA-array in pUC57-Simple | N/A | Synthetized by Genescript, with linker GSGSG and codon optimized |
| DNA plasmid | pMT-SuntagRLucFKBP24MS2v5-SV40 | N/A | Used in S2 cell experiments |
| DNA plasmid | pAWF-stdMCP-stdHalotag | N/A | Used in S2 cell experiments |
| DNA plasmid | pAWF-scFv-msGFP2 | N/A | Used in S2 cell experiments |
| DNA plasmid | pAWF-scFv-sfGFP | N/A | Used in S2 cell experiments |
| DNA plasmid | 12x_ALFA-array for CRISPR tagging DYNC1H1 | N/A | Used for HeLa cells experiments |
| DNA plasmid | NB-ALFA-sfGFP in pHR | N/A | Used for HeLa cells experiments |
| DNA plasmid | pAWF-anti-ALFA-msGFP2ΔGB1 | N/A | Used in S2 cell experiments |
| DNA plasmid | pAWF-anti-ALFA-msGFP2 | N/A | Used in S2 cell experiments |
| DNA plasmid | pAWF-scFv-msGFP2ΔGB1 | N/A | Used in S2 cell experiments |

| | | | |
|---|---|---|---|
| DNA plasmid | pHAGE Ubc NLS-HA MCP-tdStayGold | N/A | Used for HeLa cells experiments |

492

493

494 **Fly stocks, handling and genetics**

495 The *yw* fly stock was used as a wild type. The germline driver *nos-Gal4:VP16* (BL4937)
496 and the *His2av-mRFP* (Bl23651) fly stocks come from Bloomington Drosophila Stock
497 Center. The *nullo-Gal4* fly stock comes from R.L. laboratory. The
498 *twi_suntag_MS2_CRISPR*, *twi_suntag_transgene* and *scFv-mScarlet* lines were
499 from[7]. Briefly, the 32x suntag sequence from[4] (containing thirty-three suntag repeats)
500 was inserted in frame into *twi* gene[7] and 128X MS2 from[28] placed just after the stop
501 codon. All live experiments were done at 21 °C except when using - or comparing to -
502 strains containing UAS-GAL4 which were done at 25 °C.

503

504 **Cloning and transgenesis**

505 *scFv-FP* under *nanos* enhancer-promoter (EPr) lines were generated using
506 NEBuilder® HiFi DNA Assembly Master Mix with primers listed in supplementary table
507 1 and inserted into scFv-sfGFP vector[7] digested with BamHI/XhoI. The transgenic
508 construct was inserted into the VK00033 (BL9750) and VK00027 (BL9744) landing site
509 using PhiC31 targeted insertion[71]. *UASp-scFv-FP* lines were done by inserting
510 fragment of the scFv-FP plasmid digested with XhoI/HpaI in the UASp-scFv-sfGFP
511 vector[6] digested with XhoI/HpaI. The transgenic construct was inserted in the VK00033
512 (BL9750) landing site using PhiC31 targeted insertion[71]. Fluorescent proteins were
513 extracted from plasmids: mAvicFP1 from pNCST-mAvicFP1 (addgene 129509),
514 mGreenLantern from pcDNA3.1-mGreenLantern (addgene 161912), msGFP2
515 (addgene 160461), mNeonGreen is a kind gift from S.Piatti. The Ilp4 transgene

516 (regulatory regions and coding sequence) was synthesized (GenScript Biotech) into
517 pUC57-simple[7]. The 32x_ALFA-array repeats were synthesized (GenScript Biotech)
518 into pUC57-simple (see supplementary materials). The 32x_ALFA-array was inserted
519 between Kpn1 and EcoRV restriction sites of the Ilp4 puc57-simple vector. Ilp4-ALFA-
520 array fragment was inserted into pBPhi using PmeI and Nhe1 and injected into BL9750
521 using PhiC31 targeted insertion[71] (BestGene, Inc.). The NB-ALFA were synthesized
522 (GenScript Biotech) into pUC57-simple (see supplementary materials), then msGFP2,
523 GB1 and a NLS was added using NEBuilder® HiFi DNA Assembly Master Mix with
524 primers listed in supplementary table 1 and inserted into scFv-sfGFP vector[7] digested
525 with BamHI/XhoI. The transgenic construct was inserted into the VK00033 (BL9750)
526 landing site using PhiC31 targeted insertion[71]. All cloning for plasmids used in
527 *Drosophila* S2 cells were performed using In-Fusion® HD Cloning Plus Kit (Takara
528 Bio) and PCR was carried out with CloneAmp HiFi PCR premix (Takara Bio). Primers
529 used are listed in supplementary table 1. To inducibly express SunTag in S2 cells, we
530 generated pMT-SuntagRLucFKBP24MS2v5-SV40 by inserting
531 SuntagRLucFKBP24MS2v5 fragment (addgene 119946) into pMT backbone that was
532 PCR-amplified from pMT-EGFPActin5C (addgene 15312) with In-Fusion® HD Cloning
533 Plus Kit. For constitutive expression in S2 cells, pAWF (DGRC stock # 1112) was used
534 as an expression vector. pAWF-stdMCP-stdHalotag was generated by inserting
535 stdMCP-stdHalotag (addgene 104999) into PCR-linearized pAWF vector using In-
536 Fusion® HD Cloning Plus Kit. To generate pAWF-scFv-FPs, sequences containing
537 scFv fused to various fluorescent proteins and GB1-NLS were amplified from *scFv-FP*
538 under *nanos* enhancer promoter plasmids generated in this article and ligated with
539 PCR-linearized pAWF vector using In-Fusion® HD Cloning Plus Kit. All plasmid
540 sequences are listed in supplementary materials. The sequence of anti-ALFA-

541 msGFP2-GB1-NLS was inserted into pAWF vector (DGRC #1112) to generate plasmid
542 pAWF-anti-ALFA-msGFP2. To remove GB1 and generate pAWF-anti-ALFA-msGFP2
543 ΔGB1, a pair of primers flanking the GB1 sequence were used to amplify the entire
544 pAWF-anti-ALFA-msGFP2 sequence except for the GB1 and ligated with KLD enzyme
545 mix (NEB, M0554S). Same primer pairs were used to generate pAWF-scFv-
546 msGFP2ΔGB1 from pAWF-scFv-msGFP2.
547

548 **Single molecule fluorescence *in situ* hybridization (smFISH) and immuno-**
549 **smFISH in *Drosophila***

550 A pool of 0-4h after egg-laying (AEL) embryos were dechorionated with bleach for
551 3 min and thoroughly rinsed with $H_2O$. They were fixed in 1:1 heptane:formaldehyde-
552 10% for 25 min on a shaker at 450 rpm; formaldehyde was replaced by methanol and
553 embryos were shaken by hand for 1 min. Embryos that sank to the bottom of the tube
554 were rinsed three times with methanol and kept at -20°C for further use.
555 Embryos were washed 5 min in 1:1 methanol:ethanol, rinsed twice with ethanol 100%,
556 washed 5 min twice in ethanol 100%, rinsed twice in methanol, washed 5 min once in
557 methanol, rinsed twice in PBT-RNasin (PBS 1x, 0.1% tween, RNasin® Ribonuclease
558 Inhibitors). Next, embryos were washed 4 times for 15 min in PBT-RNasin
559 supplemented with 0.5% ultrapure BSA and then once 20 min in Wash Buffer (10%
560 20X SCC, 10% Formamide). They were then incubated overnight at 37 °C in
561 Hybridization Buffer (10% Formamide, 10% 20x SSC, 400 µg/ml *E. coli* tRNA (New
562 England Biolabs), 5% dextran sulfate, 1% vanadyl ribonucleoside complex (VRC) and
563 smFISH Stellaris probes against *suntag*[7] or 32x_ALFA-array coupled to Quasar 570
564 (supplementary table 1) or probes against 32X MS2 coupled to Cy3 (from E.
565 Bertrand)[54] and/or GCN4 primary antibody (Novus Biologicals C11L34) (1/200) and/or

566 affinity purified rabbit anti-ALFA polyclonal antibody (NanoTag Biotechnologies)
567 (1/200). Probe sequences are listed in Supplementary table 1. The next day,
568 secondary antibody (1/500 anti-mouse Alexa 488-conjugated (Life Technologies,
569 A21202); anti-mouse Alexa 647-conjugated (Invitrogen, A32728); anti-rabbit Alexa
570 555-conjugated (Life Technologies, A31572) or anti-rabbit Alexa 488-conjugated (Life
571 Technologies, A21206)) was added if necessary, during 1h at 37° in Wash Buffer. DAPI
572 was added at 45min (1/1000). Embryos were then washed three times 15min in 2x
573 SCC, 0.1% Tween at room temperature before being mounted in ProLong® Diamond
574 antifade reagent.
575 Images were acquired using a Zeiss LSM880 confocal microscope with an Airyscan
576 detector in Super Resolution (SR) mode. GFP/Alexa-488 was excited using a 488 nm
577 laser, Cy3/Quasar 570 were excited using a 561 nm laser, Alexa 647 was excited using
578 a 633 nm laser. Laser powers were: 27μW for 488nm laser (9μW for UAS>nos
579 images), 80μW for 561nm laser and 46μW for 633nm laser. Laser powers were taken
580 under a 10X objective. Figures were prepared with ImageJ (National Institutes of
581 Health), Photoshop (Adobe Systems), and Illustrator (Adobe Systems).
582 Percentage of mRNA in translation and polysome intensities were quantified with
583 custom-made algorithms developed in PythonTM[7]. Quantification was done on three
584 area at the center and three area at the border of the mesoderm from three mid-late
585 embryos for *scFv-msGFP2>twi_suntag_MS2_CRISPR/+* (related to Figure 2b) and
586 three area at the center and three area at the border of the mesoderm from two mid-
587 late embryos for *twi_suntag_MS2_CRISPR/+* stained with anti-GCN4 antibody (related
588 to Figure 2e). Outliers were removed using the ROUT method[72], embedded in
589 GraphPad Prism 9.3.1 software, with Q set to 0.1%. scFv-FP intensities (related to
590 Figure S1f) were quantified using images from two to three early-mid *scFv-*

591 *FP>twi_suntag_MS2_CRISPR/+* embryos, outliers were removed using the ROUT
592 method[72], embedded in GraphPad Prism 9.3.1 software, with Q set to 0.1%.
593
594 **Cell culture**
595 Drosophila S2R+ cells (DGRC Stock 150) were maintained at 25°C in Schneider's
596 medium containing 10% Fetal Bovine Serum and 1% Penicillin-streptomycin. For the
597 transfection, 0.7x10^6 cells in 350ul were seeded into each well of a 24-well plate.
598 Cells are transfected with plasmid mix of pMT-SuntagRLucFKBP24MS2v5-SV40 or
599 pMT-ALFAx32-RLucFKBP24MS2v5-SV40 (200ng), pAWF-MCP-Halotag (5ng),
600 pAWF-scFv-FP-GB1-NLS or pAWF-scFv-FP-NLS (10ng) using effectene transfection
601 reagent. 24h after transfection, cells were first incubated with Schneider's medium
602 containing 200 nM Janelia Fluor® 594 HaloTag® Ligand (Promega GA1110) for 15min
603 and then switched to medium with 1 mM CuSO4 for 1h or 3h to induce expression of
604 pMT construct.
605 HeLa cells were maintained in DMEM supplemented with 10% FBS, 10 U/ml
606 penicillin/streptomycin and 2.9 mg/ml glutamine in a humidified $CO_2$ incubator at 37°C.
607 For translational inhibition, cells were treated with puromycin at 100 µg/ml for 30 min.
608 Cells were transfected with JetPrime (Polyplus) and selected on 150 µg/ml
609 hygromycin. For each stable cell line, several individual clones were picked and
610 screened by smFISH with sets of fluorescent oligonucleotide probes against the
611 integrated sequence. For CRISPR recombination, clones were additionally analyzed
612 by genomic PCR using amplicons specific for the non-recombined or the recombined
613 allele. The CRISPR guide and repair plasmids have been previously[4]. For the repair
614 plasmid, the 12x_ALFA-array replaced the SunTag 56x tag.

615 The NB-ALFA-sfGFP was introduced into HeLa cells by retroviral infection. HEK293T
616 cells were transiently transfected with a cocktail of plasmids coding for retroviral
617 components and producing the genomic NB-ALFA-sfGFP retroviral RNAs. Viral
618 particles were collected and used to infect recipient HeLa cells, which were then sorted
619 by FACS. Only lowly expressing cells were selected.
620 For FRAP experiment, 150k HeLa cells expressing NB-ALFA-sfGFP were seeded in
621 fluorodish 35mm. The day after, cells were transfected with a mix of 3ug of
622 H2B_mCherry_ALFAtag plasmid, 4 µl of Jet Prime Reagent and 200 µl of Jet Prime
623 Buffer. The mix was vortexed for 15 seconds and incubated at RT for 10 minutes before
624 being added to the cells. After 24h, medium containing transfection reagents was
625 washed with PBS and replaced with fresh medium. Cells were incubated for an
626 additional 24h before use. One hour before the FRAP experiment, cells were washed
627 three times with PBS, and incubated in imaging media.
628 For testing NLS-MCP-tdStaygold, stable expression of fluorescent MCP fusions was
629 achieved by lentivirus-mediated transduction of a self-inactivating vector containing an
630 internal ubiquitin promoter as described in[54]. The MCP contained the deltaFG deletion,
631 the V29I mutation, and an SV40 NLS. Cells expressing fluorescent MCP fusions were
632 grown as a pool of clones and FACS-sorted to select cell populations expressing
633 homogeneous levels of fluorescence. The reporter cell lines additionally expressed the
634 HIV-1 reporter gene pIntro-MS2x128 previously described in[54].
635
636 **Western blot**
637 S2 cells (about 10^6 cells at 3x10^6 cell/ml density) were transfected with 300ng of
638 plasmids pAWF-scFv-msGFP2, pAWF-scFv-msGFP2ΔGB1, pAWF-anti-ALFA-
639 msGFP2, pAWF-anti-ALFA-msGFP2ΔGB1, or empty pAWF vector using Effectene

640 transfection reagent (Qiagen, # 301425). Cells were harvested 48h after transfection,
641 lysed with NuPAGE™ LDS Sample Buffer (Invitrogen, NP0007), and denatured by
642 heating at 70°C for 10 min. Proteins in the lysate samples were resolved by
643 electrophoresis using NuPAGE™ 4 to 12%, Bis-Tris gel, and transferred onto a PVDF
644 membrane using Trans-Blot Turbo Transfer System (Bio-Rad). The PVDF membrane
645 was blocked using Intercept (PBS) Blocking Buffer (LI-COR, 927-70001) for 1 h before
646 being incubated with primary antibodies (rabbit anti-GFP, Invitrogen, A11122; mouse
647 anti-αTubulin, Sigma, T6199-100UL) with 1:3000 dilution overnight at 4°C. When
648 primary antibody was omitted, the membrane was incubated in the blocking buffer
649 overnight at 4°C. The membrane was extensively washed before being incubated with
650 secondary antibodies (Goat anti-Rabbit-HRP, Invitrogen 65-6120; Goat anti-Mouse-
651 HRP, sigma 12-349) at 1:3000 dilution for 1 h at room temperature. The membrane
652 was extensively washed before applying Pierce™ ECL Western Blotting Substrate
653 (Thermo Scientific 32106) and visualized in the BioRad gel imaging system.
654
655 **Single molecule fluorescence *in situ* hybridization (smiFISH) in mammalian cells**
656 Cells were grown on glass coverslips (0.17 mm), washed with PBS, fixed in 4% PFA
657 for 20 min, and permeabilized in 70% ethanol overnight at 4°C. Cells were hybridized
658 as previously described for the smiFISH procedure[73], using probes were sets of
659 unlabeled oligonucleotides hybridizing against the target RNA and additionally
660 contained a common supplementary sequence that was pre-annealed to a fluorescent
661 oligonucleotide probe termed the FLAP[73]. We used sets of oligonucleotides for the
662 DYNC1H1 mRNA[4]. Slides were mounted in Vectashield with DAPI (Vector
663 Laboratories).

664 Fixed cells were imaged at room temperature on an Axioimager Z1 wide-field
665 microscope (63×, NA 1.4; ZEISS) equipped with an sCMOs Zyla 4 0.2 camera (Andor
666 Technology) and controlled by MetaMorph (Universal Imaging). 3D image stacks were
667 collected with a Z-spacing of 0.3 µm. Figures were prepared with ImageJ (National
668 Institutes of Health), Photoshop (Adobe Systems), and Illustrator (Adobe Systems).
669

670 **Live cell imaging of mammalian cells**

671 Cells were plated on FluoroDish (35mm, FD35-100, World Precision Instruments,
672 Sarasota,FL,USA) one day before the imaging. Before imaging media was replaced
673 for imaging purpose with a non-fluorescent media (FluoroBrite DMEM, from
674 thermofischer scientific cat no.A1896701, was supplemented with 10% FBS, 1%
675 penicillin/streptomycin, 1% glutamine and rutin; Evrogen). The dish was mounted in a
676 temperature-controlled chamber with 5 % CO2 and imaged on an inverted OMXv3
677 Deltavision microscope in time-lapse mode. A 100x, NA 1.4 objective was used, with
678 an intermediate × 2 lens and an Evolve 512 × 512 EMCCD camera (Photometrics). 9
679 stacks with a z-spacing of 0.6 µm were acquired. Illuminating light and exposure time
680 were set at 1% of laser full power, exposure of 40 ms per plane. For the time-lapse
681 mode, one stack was recorded every 10s for 3h to 6h. Both the MCP-eGFP and MCP-
682 tdStaygold cell lines were imaged under the same conditions.
683

684 **Signal quantification in mammalian cells**

685 MCP fusions, quantification was performed using big-FISH, a Python-based software
686 for the analysis of RNA single molecules[74]. Spots were detected using a Laplacian of
687 Gaussian threshold and the program returned the number of the RNA molecule, mean
688 and standard deviation of the fluorescence intensity. The threshold was manually set

689 for each frame for optimal detection of single RNAs and transcription sites were
690 removed from the analysis. Background nucleoplasmic intensities from free fluorescent
691 MCP proteins was subtracted from each frame. The code for the analysis described in
692 this paper is available on GitHub: https://github.com/fish-quant.
693

694 **Fluorescence correlation spectroscopy**

695 FCS experiments were performed on a Zeiss LSM780 microscope using a 40x/1.2
696 water objective. GFP was excited using the 488 nm line of an Argon laser with a
697 constant excitation intensity. Fluorescence intensity fluctuations were acquired for 1 s
698 and auto-correlation functions (ACFs) generated by Zen software were loaded in the
699 PyCorrFit program[75] and fit using a simple 3D gaussian model:

700 $$G(\tau) = \frac{1}{N}\left(1 + \frac{\tau}{\tau_D}\right)^{-1}\left(1 + \frac{\tau}{s^2\tau_D}\right)^{-1/2} \quad (1)$$

701 With N the number of molecules, $\tau_D$ the diffusion time and s the structural parameter
702 (shape of the PSF) fixed to 5. The brightness B is obtained by dividing the average
703 value of the fluorescence intensity ($\langle F(t)\rangle$ by the number of molecules N obtained by
704 the fit of the ACF with equation (1).
705 Multiple measurements per embryo, in multiple position and embryos at 20 °C were
706 used to generate multiple ACF, used to extract brightness and molecule numbers.
707 Outliers were removed using the ROUT method[72], embedded in GraphPad Prism 9.3.1
708 software, with Q set to 0.1%.
709

710 **Fluorescence recovery after photobleaching**

711 Fluorescence recovery after photobleaching (FRAP) was performed in HeLa cells
712 expressing NB-ALFA-sfGFP wich was transfected with H2B_mCherry_ALFAtag
713 plasmid[51] and imaged 48 hours later at 37°C. The following settings was used: a Zeiss

714 LSM980 using a 40x/1.3 Oil objective. Images (512 × 512 pixels), 16bits/pixel, pixel
715 size 0.12µm, zoom 3.5x, were acquired every ≈10 s during 30 frames. Excitation: GFP
716 with a laser at 488nm and mCherry with a laser at 561nm. Laser power was measured
717 using the 40x/1.3 Oil objective at 1mW for 488nm and 561nm laser at 100% and
718 acquisition laser power was measured at 50µW and 2.2µW for 488nm and 561nm
719 diode laser respectively. A circular ROI (3.7µm diameter) was bleached using hundred
720 pulses of 488 nm and 561 lasers at maximal power (100%) after 1 pre-bleach frames.
721 To discard any source of fluorescence intensity recovery other than molecular
722 diffusion, the measured fluorescence recovery in the bleached ROI region ($I_{bl}$) was
723 corrected by an unbleached ROI ($I_{unbl}$) of the same nucleus and another ROI outside
724 of the cells ($I_{out}$) following the simple equation:

725 $$I_{blcorr}(t) = \frac{I_{bl}(t) - I_{out}(t)}{I_{unbl}(t) - I_{out}(t)} \quad (2)$$

726

727 **Light-Sheet Microscopy**

728 For light-sheet imaging (related to Movie S6-7 and Figures S1d), the MuViSPIM[76]
729 (Luxendo, Brüker company GMBH) was employed. This setup provides two-sided
730 illumination with two Nikon 10x/0.3 water objectives and two-sided detection with two
731 Olympus 20x/1.0 W objectives. The lightsheet is created by scanning a Gaussian
732 beam, as in digital scanned laser light-sheet microscopy (DSLM). We used the line
733 mode which is an in-built synchronization between rolling shutter readout mode of
734 sCMOS cameras and digital light sheets canning. This allows the rejection of out-of-
735 focus and scattered light, thus improving the signal to noise ratio. Images are acquired
736 by two ORCA Flash 4.0 (C91440) from Hamamatsu and processed by LuxControl
737 v1.10.2. A 50ms exposure time was used for the green channel with a 488nm laser.
738 Maximum intensity projections were processed with Fiji[77].

739

740 **Live imaging of the scFv-FP and NB-ALFA-msGFP2 alone**

741 For all live imaging experiments, embryos were dechorionated with tape and mounted
742 between a hydrophobic membrane and a coverslip as described previously[78].
743 Movies for scFv-FP (related to Figure S1 and Movie S1-5) and NB-ALFA-msGFP2
744 under *nanos* promoter (related to Figure S8 and Movie S23) were acquired using a
745 Zeiss LSM880 confocal microscope with a Plan-Apochromat 40x/1.3 oil objective lens,
746 with green excitation using a 488nm laser (6µw measured with 10x objective lens). A
747 GaAsP detector was used to detect fluorescence with the following settings: 512x 512-
748 pixels images, zoom 2x, each Z-stack comprised of 25 planes spaced 1µm apart.
749 Movies for *UASp>scFv-FP* (related to Figure S6, and Movie S16-19) and *UASy>scFv-*
750 *msGFP2* with *nos-Gal4* driver (related to Figure S7 and Movie S21) were acquired
751 using a Zeiss LSM880 confocal microscope with a Plan-Apochromat 40x/1.3 oil
752 objective lens, with green excitation using a 488nm laser (1µw measured with 10x
753 objective lens). A GaAsP detector was used to detect fluorescence with the following
754 settings: 512x 512-pixels images, zoom 2x, each Z-stack comprised of 25 planes
755 spaced 1µm apart.

756

757 **Live imaging of the scFv-FP and anti-ALFA-msGFP2 in presence of tagged genes**

758 For all live imaging experiments, embryos were dechorionated with tape and mounted
759 between a hydrophobic membrane and a coverslip as described previously[78].
760 Movies of *scFv-FP>twi_suntag_MS2_CRISPR/+* (related to Figure 1 and Movie S8-
761 12) were acquired using a Zeiss LSM880 with confocal microscope in fast Airyscan
762 mode with a Plan-Apochromat 40x/1.3 oil objective lens. GFP was excited using a
763 488nm (7uw measured with 10x objective lens) laser with the following settings: 132x

764 132-pixel images, each Z-stack comprised of 15 planes spaced 0.5µm apart and zoom
765 8x. Intensity measurement of each polysomes was done on a MIP of 5 planes using a
766 custom-made software written in Python, that performs a spot detection on the MIP
767 raw data stack. For each time frame, the software performs a Laplacian of Gaussian
768 2D filter and the filtered images are than thresholded with a user defined threshold.
769 The threshold is expressed in terms of the average and standard deviation of intensity
770 values of each image in order to have a threshold value self-re-scaled with respect to
771 the characteristic of the images itself. Spots smaller in size than a user-defined value
772 are removed (considered as fake detection). Finally, for each of the detected spots, we
773 use a 2D expansion of the spots silhouettes in order to define a region around the
774 spots devoided of any other spots and that we can use to estimate background and
775 measure it all along the time evolution for corrections purposes.
776 Movies of *scFv-FP>twi_suntag_MS2_CRISPR/+* and *scFv-*
777 *msGFP2>twi_suntag_transgene* (related to Figure 2, Figure S4 and Movie S13-15)
778 were acquired using a Zeiss LSM880 with confocal microscope in fast Airyscan mode
779 with a Plan-Apochromat 40x/1.3 oil objective lens. GFP was excited using a 488nm
780 (4.7µW measured with 10x objective lens) laser with the following settings: 568x 568-
781 pixel images, each Z-stack comprised of 61 planes spaced 0.5µm apart and zoom 2x.
782 Movies were then processed to remove frame outside of the embryos or containing the
783 membrane signal to correct drifting, and processed stacks were maximum intensity
784 projected using custom-made software, developed in Python™[7].
785 Movies of *nos-Gal4>UASp-scFv-msGFP2* x *twi_suntag_MS2_CRISPR/+* and *scFv-*
786 *msGFP2* x *twi_suntag_MS2_CRISPR/+* (related to Figure 3e and Movie S20) were
787 acquired using a Zeiss LSM880 with confocal microscope in fast Airyscan mode with
788 a Plan-Apochromat 40x/1.3 oil objective lens. GFP was excited using a 488nm (5uw

789 measure with 10x objective lens) laser with the following settings: 396x 396-pixel
790 images, each Z-stack comprised of 30 planes spaced 0.5µm apart and zoom 4x.
791 Live tilescans of *nullo-Gal4*>UASy-*scFv-msGFP2-NLS* (related to Movie S22) were
792 acquired using a Zeiss LSM880 with confocal microscope in fast Airyscan mode with
793 a Plan-Apochromat 40x/1.3 oil objective lens. GFP was excited using a 488nm (13µW
794 measured with 10x objective lens) laser with the following settings: 1440 x 2746-pixel
795 images using two tiles, each Z-stack comprised of 9 planes spaced 2µm apart and
796 zoom 0.8x.
797 Live tilescans of *UASy-scFv-msGFP2-NLS/ his2Av-RFP* in presence or not of *nullo-*
798 *Gal4* driver (related to Supplementary Figure S7d) were acquired using a Zeiss
799 LSM880 with confocal microscope in fast Airyscan mode with a Plan-Apochromat
800 40x/1.3 oil objective lens. GFP was excited using a 488nm (13µW measured with 10x
801 objective lens) and RFP was excited using a 561nm laser with the following settings:
802 1024 x 3072-pixel images using three tiles, each Z-stack comprised of 14 planes
803 spaced 2µm apart.
804 Movies of NB-ALFA-msGFP2 under *nanos* EPr crossed with *Ilp4_32x_ALFA-array*
805 (related to Figure 4e and Movie S24) were acquired using a Zeiss LSM880 with
806 confocal microscope in fast Airyscan mode with a Plan-Apochromat 40x/1.3 oil
807 objective lens. GFP was excited using a 488nm (6.4µW measured with 10x objective
808 lens) laser with the following settings: 256x 256-pixel images, each Z-stack comprised
809 of 6 planes spaced 1µm apart and zoom 6x.
810 Live tilescans of NB-ALFA-msGFP2 under *nanos* EPr crossed with *Ilp4_32x_ALFA-*
811 *array* (related to Figure S8e-f and Movie S25) were acquired using a Zeiss LSM880
812 with confocal microscope in fast Airyscan mode with a Plan-Apochromat 40x/1.3 oil
813 objective lens. GFP was excited using a 488nm (13µW measured with 10x objective

814 lens) laser with the following settings: 1612 x 4860-pixel images using 3 tiles, each Z-
815 stack comprised of 9 planes spaced 2µm apart.
816 Movies of *NB-ALFA-msGFP2*, *scFv-mScarlet*, *twi_suntag_MS2_CRISPR* crossed with
817 *Ilp4_32x_ALFA-array* (related to Figure 4i and Movie S26) and NB-ALFA-msGFP2,
818 scFv-mScarlet crossed with *Ilp4_32x_ALFA-array* (related to Figure S10b and Movie
819 S27) were acquired using a Zeiss LSM880 with confocal microscope in fast Airyscan
820 mode with a Plan-Apochromat 40x/1.3 oil objective lens. GFP and mScarlet were
821 excited using a 488nm and 561nm laser respectively with the following settings: 372x
822 372-pixel images, one Z-plane and zoom 6x.
823
824 **S2 cell culture imaging**
825 Cells were pipetted into a µ-Slide (Ibidi #80621) and live-imaged using a Zeiss LSM980
826 confocal microscope with an Airyscan detector in SR mode with a 63X Plan-
827 Apochromat (1.4NA) oil objective lens. GFP was excited using a 488nm laser and
828 MCP-Halotag labelled by Janelia Fluor® 594 was excited using a 561nm laser. Cells
829 with mRNAs visible in cytoplasm and with comparable GFP signal were chosen for
830 acquiring images. Images of individual cells were acquired with following setting: z-
831 stack of 5 planes with 0.5um interval, 8x zoom, 396x396 pixel and 8 bit per pixel. GFP
832 foci co-localized with mRNA foci (Janelia Fluor® 594 signal) were considered as
833 translation sites while GFP foci or larger amorphous or ring-like GFP structures that
834 were not co-localized with mRNA were considered as aggregates.
835
836 **Acknowledgments**
837 We are grateful to NanoTag Biotechnologies for sharing ALFA-Tag and anti-ALFA
838 nanobody plasmids and advices. We are grateful to Dr. Karim Mazjoub's lab for sharing

space in his experimental room. We thank Drs. Xavier Pichon and Dr. Vera Slaninova for their help in setting up the mammalian ALFA-Tag system and Dr. Vera Slaninova for helping developing the MCP-tdStaygold fusion. For imaging, we acknowledge Sylvain de Rossi and Montpellier Ressources Imagerie (MRI), a microscopy facility of The National Infrastructure France-BioImaging (FBI), supported by the French National Research Agency (ANR-10-INBS-04). We acknowledge M. Verbrugghe for help with fly handling, and the Montpellier *Drosophila* Facility (BioCampus). We thank Dr. Radhan Ramadass for assistance with software. We acknowledge Dr Etienne Schwob and Dr. Eric Kremer for their help in preparing the manuscript. We acknowledge HFSP (CDA Grant to M.L.) for the early sponsoring of the implementation of *Drosophila* translation imaging project. Funding: This work was supported by the ERC SyncDev starting grant to M.L., the ANR MemoRNP to M.L., and by IGMM internal capital, D.A. was granted by the CNRS consortium GDR ImaBio. M.L., J.D., E.B. and C.F. are sponsored by CNRS. M.B. was supported by a FRM fellowship and then by ERC SyncDev. H.L was supported by ERC SyncDev. J.Dh. was supported by ANR grant ULTIM. E.B. was supported by grants from MSDAvenir and ANR ULTIM.

**Author contributions:**

J.D. conceived the project. J.D. conceptually supervised the work with the help of M.L. at its early stages. J.D., M.B., M.L., E.B., R.L. and R.C. designed the experiments. J.D., M.B., and C.F. performed *Drosophila* embryos experiments. A.T. developed software. H.L. helped with cloning and fly handling. M.L. acquired funding. E.B. supervised mammalian cells experiments, which were performed by J.Dh.. R.L. supervised *Drosophila* S2 cells experiments performed by R.C.. J.D., M.B., R.C., A.T. E.B. and C.F. analyzed and interpreted the results. C.F. analyzed and supervised FCS

experiments with the help of J.D and M.B. J.D. and M.B. wrote the manuscript. M.L., R.C., E.B., R.L. and C.F. edited the manuscript. H.K., F.M. and E.B. developed MCP-tdStaygold fusion. E.B. and J.Dh. developed the mammalian ALFA tag system. J.D., M.B., R.C., D.A., H.K., F.M and J.Dh. performed all experiments done for the review process. All authors discussed and approved the manuscript.

**Competing interests:**

The authors declare that they have no competing interests.

**Data and materials availability:**

All relevant data supporting the key findings of this study are available within the article and its Supplementary Information files or from the corresponding author upon reasonable request. The intensity measurement software is available through this link: https://github.com/ant-trullo/Av_Ints_software/. *Drosophila* stocks will be deposited to VDRC stock center and can be asked to M.L. (mounia.lagha@igmm.cnrs.fr). Materials used for S2 cell experiments can be asked to R.L. (lehmann@wi.mit.edu). Materials used for mammalian cell experiments can be asked to E.B. (edouard.bertrand@igh.cnrs.fr).

**References:**


1. Yan, X., Hoek, T. A., Vale, R. D. & Tanenbaum, M. E. Dynamics of Translation of Single mRNA Molecules In Vivo. *Cell* **165**, 976–989 (2016).
2. Wang, C., Han, B., Zhou, R. & Zhuang, X. Real-Time Imaging of Translation on Single mRNA Transcripts in Live Cells. *Cell* **165**, 990–1001 (2016).
3. Morisaki, T. *et al.* Real-time quantification of single RNA translation dynamics in living cells. *Science (1979)* **352**, 1425–1429 (2016).
4. Pichon, X. *et al.* Visualization of single endogenous polysomes reveals the dynamics of translation in live human cells. *J Cell Biol* **214**, 769–781 (2016).
5. Wu, B., Eliscovich, C., Yoon, Y. J. & Singer, R. H. Translation dynamics of single mRNAs in live cells and neurons. *Science (1979)* **352**, 1430–1435 (2016).

894 6. Formicola, N. *et al.* Tyramine induces dynamic RNP granule remodeling and
895 translation activation in the Drosophila brain. *Elife* **10**, (2021).
896 7. Dufourt, J. *et al.* Imaging translation dynamics in live embryos reveals spatial
897 heterogeneities. *Science (1979)* **372**, 840–844 (2021).
898 8. Vinter, D. J., Hoppe, C., Minchington, T. G., Sutcliffe, C. & Ashe, H. L. Dynamics of
899 hunchback translation in real-time and at single-mRNA resolution in the Drosophila
900 embryo. *Development* **148**, (2021).
901 9. Lecerf, J.-M. *et al.* Human single-chain Fv intrabodies counteract *in situ* huntingtin
902 aggregation in cellular models of Huntington's disease. *Proceedings of the National*
903 *Academy of Sciences* **98**, 4764–4769 (2001).
904 10. Wörn, A. *et al.* Correlation between in vitro stability and in vivo performance of anti-
905 GCN4 intrabodies as cytoplasmic inhibitors. *J Biol Chem* **275**, 2795–2803 (2000).
906 11. Colby, D. W. *et al.* Development of a human light chain variable domain (V(L))
907 intracellular antibody specific for the amino terminus of huntingtin via yeast surface
908 display. *J Mol Biol* **342**, 901–912 (2004).
909 12. Tanenbaum, M. E., Gilbert, L. A., Qi, L. S., Weissman, J. S. & Vale, R. D. A protein-
910 tagging system for signal amplification in gene expression and fluorescence imaging.
911 *Cell* **159**, 635–646 (2014).
912 13. Chouaib, R. *et al.* A Dual Protein-mRNA Localization Screen Reveals
913 Compartmentalized Translation and Widespread Co-translational RNA Targeting. *Dev*
914 *Cell* **54**, 773-791.e5 (2020).
915 14. Boersma, S. *et al.* Translation and Replication Dynamics of Single RNA Viruses. *Cell*
916 **183**, 1930-1945.e23 (2020).
917 15. Bruurs, L. J. M. *et al.* Heterogeneity in viral replication dynamics shapes the antiviral
918 response. *bioRxiv* 2022.06.08.495262 (2022) doi:10.1101/2022.06.08.495262.
919 16. Boersma, S. *et al.* Multi-Color Single-Molecule Imaging Uncovers Extensive
920 Heterogeneity in mRNA Decoding. *Cell* **178**, 458-472 e19 (2019).
921 17. Safieddine, A. *et al.* A choreography of centrosomal mRNAs reveals a conserved
922 localization mechanism involving active polysome transport. *Nat Commun* **12**, 1352
923 (2021).
924 18. Chalfie, M., Tu, Y., Euskirchen, G., Ward, W. W. & Prasher, D. C. Green fluorescent
925 protein as a marker for gene expression. *Science* **263**, 802–805 (1994).
926 19. Prasher, D. C., Eckenrode, V. K., Ward, W. W., Prendergast, F. G. & Cormier, M. J.
927 Primary structure of the Aequorea victoria green-fluorescent protein. *Gene* **111**, 229–
928 233 (1992).
929 20. Zacharias, D. A., Violin, J. D., Newton, A. C. & Tsien, R. Y. Partitioning of lipid-
930 modified monomeric GFPs into membrane microdomains of live cells. *Science (1979)*
931 **296**, (2002).
932 21. Rodriguez, E. A. *et al.* The Growing and Glowing Toolbox of Fluorescent and
933 Photoactive Proteins. *Trends Biochem Sci* **42**, 111–129 (2017).
934 22. Lambert, G. G. *et al.* Aequorea's secrets revealed: New fluorescent proteins with
935 unique properties for bioimaging and biosensing. *PLoS Biol* **18**, (2020).
936 23. Bindels, D. S. *et al.* mScarlet: a bright monomeric red fluorescent protein for cellular
937 imaging. *Nat Methods* **14**, 53–56 (2017).
938 24. Leake, M. C. & Quinn, S. D. A guide to small fluorescent probes for single-molecule
939 biophysics. *Chemical Physics Reviews* **4**, 011302 (2023).
940 25. Bertrand, E. *et al.* Localization of ASH1 mRNA particles in living yeast. *Mol Cell* **2**,
941 437–445 (1998).

26. Fusco, D. *et al. Single MRNA Molecules Demonstrate Probabilistic Movement in Living Mammalian Cells HHS Public Access Author Manuscript*. *Curr Biol* vol. 13 http://images.cellpress.com/supmat/supmatin.htm. (2003).
27. Forrest, K. M. & Gavis, E. R. Live imaging of endogenous RNA reveals a diffusion and entrapment mechanism for nanos mRNA localization in Drosophila. *Curr Biol* **13**, 1159–1168 (2003).
28. Tantale, K. *et al.* A single-molecule view of transcription reveals convoys of RNA polymerases and multi-scale bursting. *Nat Commun* (2016) doi:10.1038/ncomms12248.
29. Tutucci, E. *et al.* An improved MS2 system for accurate reporting of the mRNA life cycle. *Nat Methods* **15**, 81–89 (2018).
30. Hocine, S., Raymond, P., Zenklusen, D., Chao, J. A. & Singer, R. H. Single-molecule analysis of gene expression using two-color RNA labeling in live yeast. *Nat Methods* **10**, 119–121 (2013).
31. Weil, T. T., Parton, R. M. & Davis, I. Making the message clear: visualizing mRNA localization. *Trends Cell Biol* **20**, 380–390 (2010).
32. Pichon, X., Robert, M.-C., Bertrand, E., Singer, R. H. & Tutucci, E. New Generations of MS2 Variants and MCP Fusions to Detect Single mRNAs in Living Eukaryotic Cells. *Methods Mol Biol* **2166**, 121–144 (2020).
33. Wörn, A. *et al.* Correlation between in vitro stability and in vivo performance of anti-GCN4 intrabodies as cytoplasmic inhibitors. *J Biol Chem* **275**, 2795–2803 (2000).
34. Donahue, C. E. T., Siroky, M. D. & White, K. A. An Optogenetic Tool to Raise Intracellular pH in Single Cells and Drive Localized Membrane Dynamics. *J Am Chem Soc* **143**, (2021).
35. Tanenbaum, M. E., Gilbert, L. A., Qi, L. S., Weissman, J. S. & Vale, R. D. A protein-tagging system for signal amplification in gene expression and fluorescence imaging. *Cell* **159**, 635–646 (2014).
36. Chen, D. & McKearin, D. M. A discrete transcriptional silencer in the bam gene determines asymmetric division of the Drosophila germline stem cell. *Development* **130**, 1159–1170 (2003).
37. Ali, I. *et al.* Cis-regulatory elements affecting the Nanos gene promoter in the germline stem cells. *J Biotechnol* **145**, 323–329 (2010).
38. Doren, M. Van, Williamson, A. L. & Lehmann, R. Regulation of zygotic gene expression in Drosophila primordial germ cells. *Current Biology* **8**, 243–246 (1998).
39. Garcia, H. G., Tikhonov, M., Lin, A. & Gregor, T. Quantitative Imaging of Transcription in Living Drosophila Embryos Links Polymerase Activity to Patterning. *Current Biology* (2013) doi:10.1016/j.cub.2013.08.054.
40. Pédelacq, J. D., Cabantous, S., Tran, T., Terwilliger, T. C. & Waldo, G. S. Engineering and characterization of a superfolder green fluorescent protein. *Nat Biotechnol* **24**, (2006).
41. Valbuena, F. M. *et al.* A photostable monomeric superfolder green fluorescent protein. *Traffic* **21**, (2020).
42. Campbell, B. C. *et al.* mGreenLantern: a bright monomeric fluorescent protein with rapid expression and cell filling properties for neuronal imaging. *Proc Natl Acad Sci U S A* **117**, (2020).
43. Shaner, N. C. *et al.* A bright monomeric green fluorescent protein derived from Branchiostoma lanceolatum. *Nat Methods* **10**, (2013).
44. Pan, D. J., Huang, J. D. & Courey, A. J. Functional analysis of the Drosophila twist promoter reveals a dorsal-binding ventral activator region. *Genes Dev* **5**, 1892–1901 (1991).

45. Brogiolo, W. *et al.* An evolutionarily conserved function of the drosophila insulin receptor and insulin-like peptides in growth control. *Current Biology* **11**, (2001).
46. Ivorra-Molla, E. *et al.* A monomeric StayGold fluorescent protein. *Nature Biotechnology 2023* 1–4 (2023) doi:10.1038/s41587-023-02018-w.
47. Rørth, P. Gal4 in the Drosophila female germline. *Mech Dev* **78**, 113–118 (1998).
48. Brand, A. H. & Perrimon, N. Targeted gene expression as a means of altering cell fates and generating dominant phenotypes. *Development* **118**, 401–415 (1993).
49. DeLuca, S. Z. & Spradling, A. C. Efficient Expression of Genes in the Drosophila Germline Using a UAS Promoter Free of Interference by Hsp70 piRNAs. *Genetics* **209**, 381–387 (2018).
50. Götzke, H. *et al.* The ALFA-tag is a highly versatile tool for nanobody-based bioscience applications. *Nat Commun* **10**, 4403 (2019).
51. Alessandra Vigano, M. *et al.* Protein manipulation using single copies of short peptide tags in cultured cells and in Drosophila melanogaster. *Development (Cambridge)* **148**, (2021).
52. Mueller, F., Morisaki, T., Mazza, D. & McNally, J. G. Minimizing the Impact of Photoswitching of Fluorescent Proteins on FRAP Analysis. *Biophys J* **102**, 1656 (2012).
53. Hirano, M. *et al.* A highly photostable and bright green fluorescent protein. *Nat Biotechnol* **40**, 1132–1142 (2022).
54. Tantale, K. *et al.* Stochastic pausing at latent HIV-1 promoters generates transcriptional bursting. *Nat Commun* **12**, 4503 (2021).
55. Lambert, T. J. FPbase: a community-editable fluorescent protein database. *Nature Methods 2019 16:4* **16**, 277–278 (2019).
56. Zhang, H. *et al.* Quantitative assessment of near-infrared fluorescent proteins. *Nature Methods 2023 20:10* **20**, 1605–1616 (2023).
57. Cranfill, P. J. *et al.* Quantitative assessment of fluorescent proteins. *Nat. Methods* **13**, 557–562 (2016).
58. Schneider, K. L., Wollman, A. J. M., Nyström, T. & Shashkova, S. Comparison of endogenously expressed fluorescent protein fusions behaviour for protein quality control and cellular ageing research. *Sci Rep* **11**, (2021).
59. Botman, D., de Groot, D. H., Schmidt, P., Goedhart, J. & Teusink, B. In vivo characterisation of fluorescent proteins in budding yeast. *Scientific Reports 2019 9:1* **9**, 1–14 (2019).
60. Heppert, J. K. *et al.* Comparative assessment of fluorescent proteins for in vivo imaging in an animal model system. *Mol. Biol. Cell* **27**, 3385–3394 (2016).
61. Song, S.-J., Diao, H.-P., Moon, B., Yun, A. & Hwang, I. The B1 Domain of Streptococcal Protein G Serves as a Multi-Functional Tag for Recombinant Protein Production in Plants. *Front Plant Sci* **13**, (2022).
62. Bothma, J. P., Norstad, M. R., Alamos, S. & Garcia, H. G. LlamaTags: A Versatile Tool to Image Transcription Factor Dynamics in Live Embryos. *Cell* **173**, 1810-1822.e16 (2018).
63. Dong, J. & Ueda, H. Recent Advances in Quenchbody, a Fluorescent Immunosensor. *Sensors (Basel)* **21**, 1–18 (2021).
64. Bruurs, L. J. M. *et al.* Antiviral responses are shaped by heterogeneity in viral replication dynamics. *Nat Microbiol* **8**, (2023).
65. Mateju, D. *et al.* Single-Molecule Imaging Reveals Translation of mRNAs Localized to Stress Granules. *Cell* **183**, 1801-1812.e13 (2020).
66. Ramat, A. *et al.* The PIWI protein Aubergine recruits eIF3 to activate translation in the germ plasm. *Cell Res* **30**, 421–435 (2020).

1041 67. Kang, J.-Y. *et al.* LLPS of FXR1 drives spermiogenesis by activating translation of
1042 stored mRNAs. *Science (1979)* **377**, eabj6647 (2022).
1043 68. Liu, Y. *et al.* Visualizing looping of two endogenous genomic loci using synthetic zinc-
1044 finger proteins with anti-FLAG and anti-HA frankenbodies in living cells. *Genes to*
1045 *Cells* **26**, 905 (2021).
1046 69. Zhao, N. *et al.* A genetically encoded probe for imaging nascent and mature HA-tagged
1047 proteins in vivo. *Nature Communications 2019 10:1* **10**, 1–16 (2019).
1048 70. Koch, A., Aguilera, L., Morisaki, T., Munsky, B. & Stasevich, T. J. Quantifying the
1049 dynamics of IRES and cap translation with single-molecule resolution in live cells. *Nat*
1050 *Struct Mol Biol* **27**, 1095–1104 (2020).
1051 71. Venken, K. J. T., He, Y., Hoskins, R. A. & Bellen, H. J. P[acman]: A BAC transgenic
1052 platform for targeted insertion of large DNA fragments in D. melanogaster. *Science*
1053 *(1979)* **314**, 1747–1751 (2006).
1054 72. Motulsky, H. J. & Brown, R. E. Detecting outliers when fitting data with nonlinear
1055 regression - A new method based on robust nonlinear regression and the false
1056 discovery rate. *BMC Bioinformatics* **7**, 1–20 (2006).
1057 73. Tsanov, N. *et al.* SmiFISH and FISH-quant - A flexible single RNA detection approach
1058 with super-resolution capability. *Nucleic Acids Res* **44**, (2016).
1059 74. Imbert, A. *et al.* FISH-quant v2: a scalable and modular tool for smFISH image
1060 analysis. *RNA* **28**, 786–795 (2022).
1061 75. Muller, P., Schwille, P. & Weidemann, T. PyCorrFit-generic data evaluation for
1062 fluorescence correlation spectroscopy. *Bioinformatics* **30**, 2532–2533 (2014).
1063 76. Krzic, U., Gunther, S., Saunders, T. E., Streichan, S. J. & Hufnagel, L. Multiview light-
1064 sheet microscope for rapid in toto imaging. *Nat Methods* **9**, 730–733 (2012).
1065 77. Schindelin, J. *et al.* Fiji: an open-source platform for biological-image analysis. *Nat*
1066 *Methods* **9**, 676–682 (2012).
1067 78. Dufourt, J. *et al.* Temporal control of gene expression by the pioneer factor Zelda
1068 through transient interactions in hubs. *Nat Commun* **9**, (2018).
1069

1070

1071

1072

1073 **Figure legends**

1074

1075 **Figure 1: Generation of different scFv-Fluorescent proteins (scFv-FP) to monitor**

1076 **nascent translation in *Drosophila*.**

1077 **a.** Schematic of the SunTag system. Once the mRNA (black) is translated by the

1078 ribosomes (grey), the suntag epitopes (light blue) will be bound by the single chain

1079 variable fragment (scFv) (dark blue) fused to a fluorescent protein (FP) (green).

1080 Therefore, the nascent peptide will be detected by the accumulation of fluorescent
1081 signal.
1082 **b.** (top) Schematic of the different constructs of scFv-FP generated in this study. scFv-
1083 msGFP2, scFv-GreenLantern, scFv-mAvic1 and scFv-NeonGreen were created for
1084 this study and scFv-sfGFP in our previous study[7]. (bottom) Schematic of the
1085 CRISPR/Cas9 targeted insertion strategy to obtain endogenous *twist* gene tagged with
1086 suntag and 128xMS2[7].
1087 **c.** (top) Schematic of a sagittal view of a *Drosophila* embryo with *twi* expression pattern
1088 in purple. Anterior side is on the left, posterior on the right, dorsal on the top and ventral
1089 side on the bottom. Black square represents the imaged area of the bottom panels.
1090 (bottom) One Z-plane of confocal images from smFISH with direct fluorescent protein
1091 signal in green (scFv-msGFP2, scFv-GreenLantern, scFv-mAvic1, scFv-NeonGreen
1092 and scFv-sfGFP) and *MS2* probes (red) on *scFv-FP x twi_suntag_MS2_CRISPR*
1093 embryos in early-mid n.c. 14. Scale bar are 5µm.
1094 **d.** Snapshots from representative fast-mode acquired confocal movies of
1095 *twi_suntag_MS2_CRISPR/+* embryos carrying either scFv-msGFP2, scFv-
1096 GreenLantern, scFv-mAvic1, scFv-NeonGreen or scFv-sfGFP proteins. Green dots
1097 represent nascent translation of *twi*. Scale bars are 5µm. (See related Movies S8-12).
1098 **e.** Quantification across time during n.c. 14 of different scFv-FP signals from movies
1099 represented in (d), n=5 movies from at least 3 embryos for each scFv-FP. Error bars
1100 represent SEM.
1101
1102 **Figure 2: scFv-FP concentration under *nos* EPr creates an artefactual**
1103 **translation arrest of endogenous *twi* mRNA during early embryogenesis**

1104 **a.** Schematic of nuclear elongation and cellularization during n.c. 14. In this study, we
1105 defined one early-mid stage (corresponding to 0 to 35min of the n.c. 14 from the
1106 mitosis) and one mid-late stage (corresponding to 35 to 55min of the n.c. 14 from the
1107 mitosis).
1108 **b.** (top) Schematic of a sagittal view of a *Drosophila* embryo with *twi* expression pattern
1109 in purple. Anterior side is on the left, posterior on the right, dorsal on the top and ventral
1110 side on the bottom. Black square represents the imaged area of the bottom panels.
1111 (bottom) A single Z-plane of confocal images from smFISH with direct fluorescent
1112 protein signal in green (scFv-msGFP2) and *MS2* probes (red) on *scFv-msGFP2 x*
1113 *twi_suntag_MS2_CRISPR* embryos at mid-late n.c. 14. Gray squares represent the
1114 zoomed images in the right panels. The two different zoomed images represent border
1115 (top) and internal (bottom) zone of the imaged pattern. Scale bars are 10µm on the
1116 larger images, and 5µm on the zoomed images. Staging is given by DAPI staining on
1117 a sagittal view of the imaged embryo (black and white image at the bottom).
1118 Quantification of the scFv-msGFP2 signal intensity on single molecule mRNA at the
1119 border at mid-late n.c. 14 stage (dark green, 9 images from three embryos, n=2570)
1120 and center (light green, 9 images from three embryos, n=2737) of the mesoderm is
1121 represented on the right.
1122 **c.** Schematic representing *twi_suntag_MS2_CRISPR* mRNA expression from n.c. 13
1123 to late n.c. 14 in red. From the observations on *twi* CRISPR translation (b), two
1124 hypotheses can be considered. Hypothesis 1 is that the decrease of translation
1125 observed at mid-late n.c. 14 is due to an active repression of translation. Hypothesis 2
1126 is that the amount of scFv-FP becomes limiting at mid-late n.c. 14, leading to an arrest
1127 of the detected green signal. These two hypotheses are represented in the context of
1128 *twi_suntag_MS2_CRISPR* expression (above) and *twi_suntag_transgene* expression

1129 (below). *twi_suntag_transgene* mRNA is expressed more stochastically and later than
1130 *twi_suntag_MS2_CRISPR* mRNA. In hypothesis 1, a decrease of translation should
1131 be simultaneously observed for the two constructs (mid-late n.c. 14). In hypothesis 2,
1132 no arrest of translation should be observed with *twi_suntag_transgene* as the amount
1133 of mRNA is lower.

1134 **d.** Snapshots each 15 minutes from movies of *scFv-msGFP2 x*
1135 *twi_suntag_MS2_CRISPR* or *scFv-msGFP2 x twi_suntag_transgene* embryos on the
1136 ventral side. T0 correspond to early n.c.14. White squares represent the zoomed
1137 images in the center of the panel. Note a persistence of translation for the
1138 *twi_suntag_transgene* at T0+45min (white arrowhead), absent in
1139 *twi_suntag_MS2_CRISPR* embryos. Scale bars are 10µm on the larger images, and
1140 5µm on the zoomed images. (See related Movies S13-14).

1141 **e.** (top) Schematic of a sagittal view of a *Drosophila* embryo with *twi* expression pattern
1142 in purple. Anterior side is on the left, posterior on the right, dorsal on the top and ventral
1143 side on the bottom. Black square represents the imaged area of the bottom panels.
1144 (bottom) Single Z-planes of confocal images from immuno-smFISH with anti-GCN4
1145 antibody (cyan) and MS2 probes (red) on *twi_suntag_MS2* embryos at mid-late n.c.
1146 14. Gray squares represent the zoomed images in the right panels. The two different
1147 zoomed images represent border (top square) and internal (bottom square) zone of
1148 the imaged pattern. Scale bars are 10µm on the larger images, and 5µm on the
1149 zoomed images. Staging is given by DAPI staining on a sagittal view of the imaged
1150 embryo (black and white image at the bottom). Quantification of the anti-GCN4 signal
1151 intensity on single molecule mRNA at the border (dark blue, 6 images from two
1152 embryos, n=3211) and center (light blue, 6 images from two embryos, n=4001) at mid-
1153 late n.c. 14 stage of the mesoderm is represented on the right.

1154

1155 **Figure 3: Increasing scFv-FP expression allows translation detection at later**
1156 **stages**

1157 **a.** Schematic of *UASp-scFv-msGFP2* construct and activation by the Gal4 protein. 10
1158 UAS sequences (purple) are placed upstream the P-promoter (blue) and scFv-
1159 msGFP2 (green) sequences. Gal4 proteins (yellow) will bind the UAS sequences to
1160 activate transcription of the scFv-msGFP2.

1161 **b.** Schematic of the expression of the *scFv-msGFP2* in *nosGal4>UASp-scFv-msGFP2*
1162 female strain during oogenesis until egg deposition.

1163 **c**. (left) Schematic of a sagittal view of a *Drosophila* embryo with *twi* expression pattern
1164 in purple. Anterior side is on the left, posterior on the right, dorsal on the top and ventral
1165 side on the bottom. Black square represents the imaged area of the right panels.
1166 Single Z-planes of confocal images from smFISH with direct scFv-msGFP2 fluorescent
1167 protein signal (green) and *MS2* probes (red) on *nosGal4>UASp-scFv-msGFP2 x*
1168 *twi_suntag_MS2_CRISPR* embryos in early, early-mid and mid-late n.c. 14. Gray
1169 squares represent the zoomed images in for each panel. Nuclei are counterstained
1170 with DAPI (grey, bottom images) for staging. Scale bars are 10μm on the larger
1171 images, and 5μm on the zoomed images.

1172 **d.** (top) Schematic of a *Drosophila* embryo on the ventral side with gastrulation furrow
1173 represented with invaginating cells. Black square represents the imaged area of the
1174 bottom panels. (bottom) Single Z-planes of confocal images from smFISH with direct
1175 scFv-msGFP2 fluorescent protein signal (green) and *MS2* probes (red) on
1176 *nosGal4>UASp-scFv-msGFP2 x twi_suntag_MS2_CRISPR* and *scFv-msGFP2 x*
1177 *twi_suntag_MS2_CRISPR* embryos at gastrulation stage and on the ventral side.

1178 Scale bars are 10µm on the larger images, and 5µm on the zoomed images. Note that
1179 translation dots are visible only with *nosGal4>UASp-scFv-msGFP2*.
1180 **e.** (top) Schematic of a *Drosophila* embryo on the ventral side with gastrulation furrow
1181 represented with invaginating cells. Black square represents the imaged area of the
1182 bottom panels. (bottom) Single Z-planes of confocal images from movie of *scFv-*
1183 *msGFP2 x yw, scFv-msGFP2 x twi_suntag_MS2_CRISPR* and *nosGal4>UASp-scFv-*
1184 *msGFP2 x twi_suntag_MS2_CRISPR* embryos at gastrulation stage (furrow
1185 represented with grey dashed line). Scale bars are 10µm. (See related Movie S20).
1186
1187
1188 **Figure 4: Development of the ALFA-array system to detect nascent translation**
1189 **in *Drosophila***
1190 **a.** Peptide sequence of one suntag with its linker (24 amino-acids) and peptide
1191 sequence of the ALFA-tag with its linker (20 amino-acids).
1192 **b.** Schematic of the scFv and the nanobody ALFA (NB-ALFA) fused to the fluorescent
1193 protein msGFP2 and their size in amino-acid (aa).
1194 **c.** Schematic of the ALFA-array system developed in this study to detect translation.
1195 32 ALFA-tag sequences were multimerized (blue amino-acid sequence) and inserted
1196 at the 5' of the gene of interest sequence (yellow). Upon translation, nanobodies ALFA
1197 fused to msGFP2 (NB-ALFA_msGFP2) will bind to the ALFA-tag peptides. As a
1198 bipartite system, the NB-ALFA is expressed under *nos* EPr fused to *msGFP2*,
1199 *Streptococcal protein G* (*GB1*) domain and a *Nuclear Localisation Signal* (*NLS*).
1200 **d.** Representation of the transgene mRNA containing 32x_ALFA-array in frame with
1201 the *insulin-like peptide 4* (*Ilp4*) gene sequence. Schematic of a sagittal view of a
1202 *Drosophila* embryo with *Ilp4* expression pattern in yellow. Anterior side is on the left,

1203 posterior on the right, dorsal on the top and ventral side on the bottom. Black square
1204 represents the imaged area of the bottom panels. One Z-plane of confocal images from
1205 smFISH with direct Nb-ALFA-msGFP2 fluorescent protein signal (green) and
1206 32x_*ALFA-array* probes (red) on *NB-ALFA_msGFP2>Ilp4_32x_ALFA-array* embryos
1207 in early-mid n.c. 14 on the ventral side. Scale bars are 10μm on the larger images, and
1208 5μm on the zoomed images.
1209 **e.** Snapshots from representative fast-mode acquired confocal movies of
1210 *Ilp4_32x_ALFA-array/+* n.c. 14 embryos carrying *NB-ALFA_msGFP2*. Bright white foci
1211 represent nascent translation of *Ilp4* transgene. Yellow squares represent zoomed
1212 images of the top panels. Nascent translation of *Ilp4* transgene is indicated by yellow
1213 arrowheads. Scale bars are 10μm on the larger images, and 2μm on the zoomed
1214 images. (See related Movies S24).
1215 **f.** Representation of the transgene mRNAs containing 32x_ALFA-array fused to *Ilp4*
1216 coding sequence or suntag fused to *twist* coding sequence used in (g) and (h).
1217 **g.** Schematic of a *Drosophila* embryo on the ventral side with *twi* expression pattern in
1218 purple and *Ilp4* in yellow. Black square represents the imaged area of the bottom
1219 panels. One Z-plane of confocal images from immuno-smFISH with anti-ALFA (green)
1220 labeling nascent translation of *Ilp4_32x_ALFA-array*, probes against *32x_ALFA-array*
1221 (red) labeling *Ilp4_32x_ALFA-array* mRNA molecules and anti-GCN4 antibody labeling
1222 nascent translation of *twi_suntag_transgene* (magenta) in n.c. 14 embryos. Scale bars
1223 are 1μm.
1224 **h.** Maximum intensity projection of a whole embryo confocal images from immuno-
1225 staining with anti-ALFA antibody (green) and anti-GCN4 antibody (magenta) on
1226 *Ilp4_32x_ALFA-array; twi_suntag_transgene* gastrulating embryo. Scale bars are
1227 100μm.

1228 **i.** Schematic of a *Drosophila* embryo on the ventral side with *twi* expression pattern in
1229 purple and *Ilp4* in yellow. Black square represents the imaged area of the bottom
1230 panels. Single Z-plane of confocal images from dual-color live imaging of
1231 *twi_suntag_MS2_CRISPR/+; NB-ALFA_msGFP2/scFv-mScarlet x Ilp4_32x_ALFA-*
1232 *array* embryos in n.c. 14. Scale bars are 1µm. (see related Movie S26).
1233 **j.** (top) Schematic of a *Drosophila* embryo on the ventral side with gastrulation furrow
1234 represented with invaginating cells. Confocal snapshots of a whole live embryo
1235 expressing *twi_suntag_MS2_CRISPR/+; NB-ALFA_msGFP2/scFv-mScarlet x*
1236 *Ilp4_32x_ALFA-array*, after gastrulation. Note the cytoplasmic staining from *Ilp4*
1237 translation (green) and nuclear staining from *twi* translation (purple). Scale bars are
1238 100µm.
1239
1240 **Figure 5: Development of the ALFA-array system to detect nascent translation**
1241 **in mammalian cells**
1242 **a.** (1) Schematic of the CRISPR/Cas9 targeted insertion strategy to obtain endogenous
1243 *DYNC1H1* gene tagged with 12X ALFA-tag. (2) Schematic of the ALFA-array system
1244 developed in mammalian cells. 12 ALFA-tag sequences were multimerized (blue
1245 amino-acid sequence) and inserted at the 5' of the gene of interest sequence
1246 (DYNC1H1, yellow). (3) The NB-ALFA is expressed under *spleen focus-forming virus*
1247 *(SFFV)* promoter fused to *sfGFP* and *Streptococcal protein G* (*GB1*) domain.
1248 **b.** Left: micrographs of HeLa cells expressing a DYNC1H1 allele endogenously tagged
1249 12x_ALFA-array tag and NB-ALFA-sfGFP, and treated (right) or not (left) with
1250 puromycin. Green: NB-ALFA-sfGFP signal; blue: DAPI. Scale bars are 5µm. Arrows:
1251 NB-ALFA-sfGFP spots. Right: quantification of the number of NB-ALFA-sfGFP spots

1252 per cell, with and without puromycin treatment. Error bars: standard deviation (n=40
1253 cells).
1254 **c.** Micrographs of HeLa cells expressing a DYNC1H1 allele endogenously tagged
1255 12x_ALFA-array tag and NB-ALFA-sfGFP, and hybridized in situ with a set of probes
1256 against DYNC1H1 mRNAs. On the merged panel: NB-ALFA-sfGFP signal (green);
1257 smFISH signals (red); DAPI (blue). Scale bar is 5µm. Arrows: DYNC1H1 polysomes.
1258 **d.** Top: schematic of the MCP fusion used to image RNA. Bottom: maximum projection
1259 intensity images of cells stably expressing MCP-tdStayGold (on the left) or MCP-eGFP
1260 (on the right). All images are taken under the same conditions on an OMX widefield
1261 microscope. Six time point are selected (0 min, 30 min, 60 min, 120 min, 150 min and
1262 180 min) and they are displayed with the same dynamic range. Red arrows point at
1263 transcription sites and green arrows point at individual RNA molecules. Scale bar:
1264 10 µm.
1265 **e.** Intensities of single RNA molecules over time. Graph shows intensities of RNA
1266 molecules (mean and s.d. error; five cells). Because of bleaching single molecule
1267 signal could no longer be detected and measured after 120 min in the case of MCP-
1268 eGFP. Note that MCP-tdStayGold and MCP-eGFP signals were acquired with the
1269 same time frame frequency (see methods).
1270 **f.** The graph shows the number of single RNA molecule detected over time using
1271 FISHquant (five cells).
1272
1273 **Figure Supp 1: Characterization of the different scFv-Fluorescent Proteins**
1274 **(scFv-FP)**
1275 **a.** Schematic of the expression pattern of scFv-FP under control of the *nanos*
1276 enhancer/promoter during *Drosophila* oogenesis.

1277 **b.** Snapshots from movies on embryos carrying scFv-sfGFP, scFv-msGFP2, scFv-
1278 GreenLantern, scFv-mAvic1 or scFv-NeonGreen in early and late n.c. 14. Scale bars
1279 are 10µm. (see related Movies S1-5).
1280 **c.** Quantification across time during n.c. 14 of the different scFv-FP signal from movies
1281 represented in (b), n=3 movies from 3 embryos for scFv-sfGFP and scFv-
1282 GreenLantern and n=4 movies from 4 embryos for scFv-msGFP2, scFv-mAvic1 and
1283 scFv-NeonGreen. Error bars represent SEM.
1284 **d.** Snapshots from light-sheet movies on embryos carrying scFv-mAvic1 or scFv-
1285 msGFP2 in n.c. 14 and at gastrulation stage. Ventral and dorsal view are represented
1286 for each embryo. Scale bars are 100µm. (See related Movies S6-7).
1287 **e.** Single Z-planes of confocal images from smFISH with direct fluorescent protein
1288 signal in green (scFv-msGFP2, scFv-GreenLantern, scFv-mAvic1, scFv-NeonGreen
1289 and scFv-sfGFP) and *MS2* probes (red) on *scFv-FP x twi_suntag_MS2_CRISPR*
1290 embryos in early-mid n.c. 14 on the ventral side. Images represent zoomed images
1291 from Figure 1c. Scale bars are 1µm.
1292 **f.** Quantification of the different scFv-FP signal intensity on single molecule mRNA
1293 (n=1646, n=3658, n=3080, n=6820, n=2924, of scFv-sfGFP, scFv-msGFP2, scFv-
1294 mAvic1, scFv-GL and scFv-NG respectively) in the mesoderm of early-mid n.c. 14
1295 embryo from immuno-smFISH (cropped area inside *twi* pattern, typical images in
1296 Figure 1c).
1297
1298 **Figure Supp 2: Localization of the tagged protein and scFv recognition by**
1299 **secondary antibody**
1300 **a.** (top) Schematic of a sagittal view of a *Drosophila* embryo with *twi* expression pattern
1301 in purple. Black square represents the imaged area of the bottom panels. Single Z-

1302 planes of confocal images from immuno-smFISH with direct fluorescent protein signal
1303 in green (scFv-msGFP2, scFv-GreenLantern, scFv-mAvic1, scFv-NeonGreen and
1304 scFv-sfGFP) and secondary anti-mouse antibody (magenta) on *scFv-FP x*
1305 *twi_suntag_MS2_CRISPR* embryos in n.c. 14 on the ventral side. Note the co-
1306 localization between the direct fluorescent protein signal and the secondary antibody
1307 signal as illustrated by the schematic on the top right. Scale bar are 1µm.
1308 **b.** (top) Schematic of a sagittal view of a *Drosophila* embryo with *twi* expression pattern
1309 in purple. Black square represents the imaged area of the bottom panels. Single Z-
1310 planes of confocal images from immuno-smFISH with MS2 probes (red) and
1311 secondary anti-mouse antibody (magenta) on *twi_suntag_MS2_CRISPR* embryos in
1312 n.c. 14 on the ventral side. Note that in absence of scFv-FP the secondary antibody
1313 does not detect any signal as illustrated by the schematic on the bottom. Scale bars
1314 are 1µm.
1315 **c.** (top) Schematic of a *Drosophila* embryo on the ventral side with gastrulation furrow
1316 represented with invaginating cells. Black square represents the imaged area of the
1317 bottom panels. (bottom) Single Z-planes of confocal images from smFISH with direct
1318 scFv-msGFP2 fluorescent protein signal (green) and *MS2* or *Ilp4* probes (red) on *scFv-*
1319 *msGFP2* > *twi_suntag_MS2_CRISPR* and *scFv-msGFP2* > *Ilp4_suntag* embryos at
1320 gastrulation stage and on the ventral side. Note a nuclear signal in
1321 *twi_suntag_trangene* embryos and a cytoplasmic signal in *Ilp4_suntag* embryos. Scale
1322 bars are 10µm.
1323
1324 **Figure Supp 3: The scFv-sfGFP can form aggregates in *Drosophila* embryos and**
1325 **S2 cells**

1326 **a.** Schematic of a *Drosophila* embryo on the ventral side with gastrulation furrow
1327 represented with invaginating cells. Black square represents the imaged area of the
1328 bottom panels. Snapshots from representative confocal movies of
1329 *twi_suntag_MS2_CRISPR/+* embryos at the gastrulation stage carrying either scFv-
1330 sfGFP, scFv-NeonGreen, scFv-mAvic1 or scFv-msGFP2 proteins. Scale bars are
1331 10µm.
1332 **b.** Schematic of a *Drosophila* embryo on the ventral side with gastrulation furrow
1333 represented with invaginating cells. Black square represents the imaged area of the
1334 bottom panels. Maximum intensity projection of 10 Z-planes of confocal images from
1335 smFISH with direct fluorescent protein signal in green (scFv-FP) and *MS2* probes (red)
1336 on *scFv-FP x twi_suntag_MS2_CRISPR* embryos at gastrulation stage on the ventral
1337 side. Grey squares represent zoomed images. Note the presence of scFv-sfGFP signal
1338 not overlapping with RNA (white arrowheads). Scale bars are 5µm.
1339 **c.** Schematic of the different constructs transfected in S2 cells. *scFv-FPs* and *tdMCP-*
1340 *stdHalotag* were placed downstream of the *Actin5C* promoter. Reporter containing
1341 suntag Renilla Luciferase (RLuc) and 24XMS2 was placed under the control of the
1342 inducible metallothionein (MT) promoter.
1343 **d.** Single Z-planes of confocal images of S2 cells expressing scFv-FPs (green) and
1344 MCP-Halotag (red) with induction of *SuntagRLuc24XMS2* reporter showing
1345 aggregation size of the scFv-FPs. A zoom on single mRNA in translation is shown on
1346 no aggregate's panels (white squares). Scale bars are 5µm.
1347 **e.** Percentage of the number of big (dark blue) and small (blue) aggregates (scFv-FP
1348 signal not colocalizing with an mRNA) and no (light blue) aggregates (scFv-FP signal
1349 colocalizing with an mRNA) in cells expressing *MCP-Halotag*, *SuntagRLuc24XMS2*
1350 reporter and *scFv-sfGFP2* or *scFv-msGFP2* (n=100 cells for each condition).

1351

1352 **Figure Supp 4: *twi* translation detection in developing embryos until gastrulation**

1353 **a.** (top) Schematic of a sagittal view of a *Drosophila* embryo with *twi* expression pattern
1354 in purple. Anterior side is on the left, posterior on the right, dorsal on the top and ventral
1355 side on the bottom. Black square represents the imaged area of the bottom panels.
1356 (bottom) A single Z-plane of confocal images from smFISH with direct fluorescent
1357 protein signal in green (scFv-mAvic1) and *MS2* probes (red) on *scFv-mAvic1 x*
1358 *twi_suntag_MS2_CRISPR* embryos at mid-late n.c. 14. Gray squares represent the
1359 zoomed images in the right panels. The two different zoomed images represent border
1360 (top square) and internal (bottom square) zone of the imaged pattern. Scale bars are
1361 10µm on the larger images, and 5µm on the zoomed images. Staging is given by DAPI
1362 staining on a sagittal view of the imaged embryo (black and white image at the bottom).

1363 **b.** (top) Schematic of a sagittal view of a *Drosophila* embryo with *twi* expression pattern
1364 in purple. Anterior side is on the left, posterior on the right, dorsal on the top and ventral
1365 side on the bottom. Black square represents the imaged area of the bottom panels.
1366 (bottom) A single Z-plane of confocal images from smFISH with direct fluorescent
1367 protein signal in green (scFv-NeonGreen) and *MS2* probes (red) on *scFv-NeonGreen*
1368 *x twi_suntag_MS2_CRISPR* embryos at mid-late n.c. 14. Gray squares represent the
1369 zoomed images in the right panels. The two different zoomed images represent border
1370 (top square) and internal (bottom square) zone of the imaged pattern. Scale bars are
1371 10µm on the larger images, and 5µm on the zoomed images. Staging is given by DAPI
1372 staining on a sagittal view of the imaged embryo (black and white image at the bottom).

1373 **c.** (top) Schematic of a sagittal view of a *Drosophila* embryo with *twi* expression pattern
1374 in purple. Anterior side is on the left, posterior on the right, dorsal on the top and ventral
1375 side on the bottom. Black square represents the imaged area of the bottom panels.

1376 (bottom) A single Z-plane of confocal images from smFISH with direct fluorescent
1377 protein signal in green (scFv-GreenLantern) and *MS2* probes (red) on *scFv-*
1378 *GreenLantern x twi_suntag_MS2_CRISPR* embryos at mid-late n.c. 14. Gray squares
1379 represent the zoomed images in the right panels. The two different zoomed images
1380 represent border (top square) and internal (bottom square) zone of the imaged pattern.
1381 Scale bars are 10µm on the larger images, and 5µm on the zoomed images. Staging
1382 is given by DAPI staining on a sagittal view of the imaged embryo (black and white
1383 image at the bottom).
1384 **d.** Snapshots each 15 minutes from movies of *scFv-msGFP2 x*
1385 *twi_suntag_MS2_CRISPR* embryos on the ventral side. T0 correspond to early n.c.14.
1386 White squares represent the zoomed images in the center of the panel. Note the
1387 absence of translation for *twi_suntag_MS2_CRISPR* at T0+45min, Scale bars are
1388 10µm on the larger images, and 5µm on the zoomed images. (See related Movies
1389 S15).
1390 **e.** Single Z-planes of confocal images from smFISH with direct fluorescent protein
1391 signal in green (scFv-msGFP2) and *suntag* probes (red) on *scFv-msGFP2 x*
1392 *twi_suntag_transgene* embryos in late n.c. 14 (top panels) and gastrulation stage
1393 (bottom panels) on the ventral side. Nuclei are counterstained with DAPI (blue). Scale
1394 bars are 10µm.
1395
1396 **Figure Supp 5: anti-GCN4 immunostaining detect translation until gastrulation**
1397 **a.** (top) Schematic of a *Drosophila* embryo on the ventral side with gastrulation furrow
1398 represented with invaginating cells. Black square represents the imaged area of the
1399 bottom panels. (bottom) Single Z-planes of confocal images from immuno-smFISH
1400 with anti-GCN4 antibody (cyan) and MS2 probes (red) on *twi_suntag_MS2_CRISPR*

1401 embryos. Grey squares represent the zoomed images in the bottom panels. Scale bars
1402 are 10µm on the larger images, and 5µm on the zoomed images.
1403
1404 **Figure Supp 6: Generation of UASp-Gal4 system to overexpress scFv-**
1405 **Fluorescent Proteins**
1406 **a.** (top) Schematic of the different constructs expressing the different scFv-FP (scFv-
1407 GreenLantern, scFv-NeonGreen, scFv-mAvic1, or scFv-msGFP2) under the control of
1408 the UASp promoter. (bottom) Snapshots from movies of embryos carrying *UASp-scFv-*
1409 *msGFP2, UASp-scFv-GreenLantern, UASp-scFv-mAvic1* or *UASp-scFv-NeonGreen*
1410 and *nosGal4* at early n.c.14 and gastrulation stage. Scale bars are 10µm. (See related
1411 Movies S16-19).
1412 **b.** Representative examples of autocorrelation function from FCS performed in
1413 embryos with nosEPr-*scFv-msGFP2* at early-mid n.c. 14 stage (green) and
1414 overexpressing the scFv-msGFP2 (*nosGal4>UASp-scFv-msGFP2*) at early-mid
1415 (purple) n.c. 14 stage. Dark curves represent fitting of the data using a diffusion model
1416 (see methods).
1417 **c.** Dot plots representing the brightness as a function of the number of molecules
1418 obtained from FCS analysis (f). In embryos with nosEPr-*scFv-msGFP2* n=120, in
1419 embryos with *nosGal4>UASp-scFv-msGFP2* n=278.
1420
1421 **Figure Supp 7: Generation of UASy-Gal4 system to express scFv-Fluorescent**
1422 **Proteins**
1423 **a.** Schematic of the two constructs UASz and UASy containing ten *UAS* with *hsp70*
1424 promoter and with *IVS-syn21* sequence (UASz) or without (UASy). Both of these
1425 constructs contain the *scFv-msGFP2*.

1426 **b.** Snapshots from movies of embryos carrying *UASy-scFv-msGFP2* and *nanos-Gal4*
1427 at early n.c.14 and gastrulation stage. Scale bars are 5µm. (See related Movies S21).
1428 **c.** (left) Schematic of a sagittal view of a *Drosophila* embryo with *twi* expression pattern
1429 in purple. Anterior side is on the left, posterior on the right, dorsal on the top and ventral
1430 side on the bottom. Black square represents the imaged area of the right panels. (right)
1431 A single Z-plane of confocal images from smFISH with direct fluorescent protein signal
1432 in green (scFv-msGFP2) and *MS2* probes (red) on *nosGal4>UASy-scFv-msGFP2 x*
1433 *twi_suntag_MS2_CRISPR* embryos in early-mid and mid-late n.c. 14. Staging is given
1434 by DAPI staining on a sagittal view of the embryo (black and white image at the
1435 bottom). Blue and white squares (border and internal zone of the pattern, respectively)
1436 represent the two different zoomed images on the right side of each panel. Scale bars
1437 are 10µm on the larger images, and 5µm on the zoomed images.
1438 **d.** Maximum intensity projected snapshots of a whole embryos confocal live tilescan
1439 expressing *UASy-scFv-msGFP2* and *Histone-H2A-RFP* (left panels) or
1440 *nulloGal4>UASy-scFv-msGFP2 and Histone-H2A-RFP* (right panels), after
1441 gastrulation. Scale bars are 100µm.
1442
1443 **Figure Supp 8: Efficient detection of *Ilp4* transgene translation with the new**
1444 **AlfaTag system**
1445 **a.** (left) Schematic of a sagittal view of a *Drosophila* embryo with *Ilp4* expression
1446 pattern in yellow. Anterior side is on the left, posterior on the right, dorsal on the top
1447 and ventral side on the bottom. (right) Maximum intensity projection of a whole embryo
1448 tilescan confocal images from immuno-smFISH with anti-ALFA antibody (green),
1449 *32x_ALFA-array* probes (red) and anti-GCN4 antibody (magenta) on *Ilp4_32x_ALFA-*
1450 *array* n.c.14 embryos. Scale bars are 100µm.

1451 **b.** (top) Schematic of a sagittal view of a *Drosophila* embryo with *Ilp4* expression
1452 pattern in yellow. Black square represents the imaged area of the bottom panels.
1453 (bottom) Single Z-planes of confocal images from immuno-smFISH with anti-ALFA
1454 antibody (green) and *32x_ALFA-array* probes (red) on *Ilp4_32x_ALFA-array* in early-
1455 mid n.c. 14 embryos at the border of *Ilp4* expression pattern. Scale bars are 10µm.
1456 **c.** (top) Schematic of a sagittal view of a *Drosophila* embryo with *Ilp4* expression
1457 pattern in yellow. Black square represents the imaged area of the bottom panels.
1458 (bottom) Single Z-planes of confocal images from immuno-smFISH with anti-ALFA
1459 antibody (green) and *32x_ALFA-array* probes (red) on *Ilp4_32x_ALFA-array* in early-
1460 mid n.c. 14 embryos to visualize single mRNA molecules in translation. Scale bars are
1461 5µm.
1462 **d.** (top) Schematic of the expression pattern of NB-ALFA under control of the *nos EPr*
1463 during *Drosophila* oogenesis. (bottom) Snapshots from movies of embryos carrying
1464 *nos>NB-ALFA-msGFP2* in n.c. 11, 12, 13 and 14. Scale bars are 10µm. (See related
1465 Movies S23).
1466 **e.** (top) Schematic of a sagittal view of a *Drosophila* embryo with *Ilp4* expression
1467 pattern in yellow. Black square represents the imaged area of the bottom panel.
1468 (bottom) Snapshots from movies of *NB-ALFA-msGFP2 x Ilp4_32x_ALFA-array*
1469 embryos in n.c. 14. The top image is a tile scan of the whole embryo and the bottom
1470 image a zoomed area represented with a white square at the border of *Ilp4* expression
1471 pattern. Note the green signal located in nuclei outside the pattern and in the cytoplasm
1472 within *Ilp4* pattern (corresponding to tagged Ilp4 proteins). Scale bars are 100µm in the
1473 tilescan and 10µm in the zoomed image. (See related Movies S25).
1474 **f.** (top) Schematic of a sagittal view of a *Drosophila* embryo with *Ilp4* expression pattern
1475 in yellow. Black square represents the imaged area of the bottom panel. (bottom)

1476 Snapshots from movies of *NB-ALFA_msGFP2 > Ilp4_32x_ALFA-array* embryos at
1477 gastrulation stage. The top image is a tile scan of the whole embryo and the bottom
1478 image a zoomed area represented with a white square at the gastrulation furrow. Scale
1479 bars are 100µm in the tilescan and 10µm in the zoomed image. (See related Movies
1480 S24).
1481
1482 **Figure Supp 9: The GB1 domain is recognized by secondary antibodies**
1483 **a.** (top) Schematic of a sagittal view of a *Drosophila* embryo with *Ilp4* expression
1484 pattern in yellow. Black square represents the imaged area of the bottom panels.
1485 Single Z-planes of confocal images from immuno-smFISH with direct fluorescent
1486 protein signal in green (NB-ALFA-msGFP2) and secondary anti-mouse antibody
1487 (magenta) on *NB-ALFA-msGFP2 x Ilp4_32x_ALFA-array* embryos in n.c. 14 on the
1488 ventral side. Note the co-localization between the direct fluorescent protein signal and
1489 the secondary antibody signal as illustrated by the schematic on the bottom. Scale bars
1490 are 1µm.
1491 **b.** (top) Schematic of a sagittal view of a *Drosophila* embryo with *Ilp4* expression
1492 pattern in yellow. Black square represents the imaged area of the bottom panels.
1493 Single Z-planes of confocal images from immuno-smFISH with ALFA probes (red) and
1494 secondary anti-mouse antibody (magenta) on *Ilp4_32x_ALFA-array* embryos in n.c. 14
1495 on the ventral side. Note that in absence of NB-ALFA the secondary antibody does not
1496 detect any signal as illustrated by the schematic on the bottom. Scale bars are 1µm.
1497 **c.** Western-blot experiments on *Drosophila* S2R+ cells transfected with scFv-msGFP2,
1498 scFv-msGFP2ΔGB1, empty vector, NB-ALFA-msGFP2 or NB-ALFA-msGFP2ΔGB1.
1499 The membrane on the left was hybridized with either anti-GFP primary and anti-rabbit
1500 secondary antibodies or with anti-rabbit secondary alone. Bands corresponding to the

1501 scFv and the NB fused to msGFP2 (with and without the GB1) are highlighted with
1502 black stars. The red stars highlight the binding of the secondary anti-rabbit-HRP to the
1503 scFv-msGFP2 and NB-msGFP2 in the presence of the GB1. The membrane on the
1504 right was hybridized with either anti-mouse secondary alone or with anti-Tubulin
1505 primary and anti-mouse secondary antibodies. The green stars highlight the binding of
1506 the secondary anti-mouse-HRP to the scFv-msGFP2 and NB-msGFP2 in the presence
1507 of the GB1.
1508
1509 **Figure Supp 10: Specificity of detection of two distinct mRNA species in fixed**
1510 **and live samples**
1511 **a.** Maximum intensity projection of a whole embryo tilescan confocal images from
1512 immuno-smFISH with anti-ALFA antibody (green), *32x_ALFA-array* probes (red) and
1513 anti-GCN4 antibody (magenta) on *Ilp4_32x_ALFA-array; twi_suntag_transgene*
1514 embryos in n.c. 14. Scale bars are 100µm.
1515 **b.** Schematic of a *Drosophila* embryo on the ventral side with *twi* expression pattern in
1516 purple and *Ilp4* in yellow. Black square represents the imaged area of the bottom
1517 panels. One Z-plane of confocal images from live imaging of *NB-ALFA_msGFP2/scFv-*
1518 *mScarlet x Ilp4_32x_ALFA-array* embryos in n.c. 14. Note the absence of signal with
1519 scFv-mScarlet illustrating specificity of the scFv and the NB-ALFA. Scale bars are 1µm
1520 (see related Movies S27).
1521 **c.** (top) Schematic of a *Drosophila* embryo on the ventral side with gastrulation furrow
1522 represented with invaginating cells. Confocal snapshots of a live embryo expressing
1523 *NB-ALFA_msGFP2/scFv-mScarlet x Ilp4_32x_ALFA-array*, after gastrulation. Scale
1524 bars are 100µm.
1525

1526 **Figure Supp 11: NB-ALFA exhibits a long binding time with its ALFA-Tag**

1527 **a.** Images from a FRAP experiment on HeLa cells expressing a NB-ALFA-sfGFP
1528 (green) and transfected with an H2B_mCherry_ALFAtag plasmid (magenta). Images
1529 before and after photobleaching are represented. The bleached area is represented
1530 with dashed white circles. Scale bars are 5µm.

1531 **b.** FRAP recovery curve from experiment in (c) of the fluorescence intensity as a
1532 function of time. Recovery of the NB-ALFA-sfGFP is in green and of the H2B in
1533 magenta.

1534

1535 **Movie Sup legends**

1536

1537 **Movie S1**: Maximum intensity projection of confocal Z-stack live imaging of an embryo
1538 containing *scFv-sfGFP*. scale bar 10µm.

1539 **Movie S2**: Maximum intensity projection of confocal Z-stack live imaging of an embryo
1540 containing *scFv-mAvic1*. scale bar 10µm.

1541 **Movie S3**: Maximum intensity projection of confocal Z-stack live imaging of an embryo
1542 containing *scFv-msGFP2*. scale bar 10µm.

1543 **Movie S4**: Maximum intensity projection of confocal Z-stack live imaging of an embryo
1544 containing *scFv-NeonGreen*. scale bar 10µm.

1545 **Movie S5**: Maximum intensity projection of confocal Z-stack live imaging of an embryo
1546 containing *scFv-GreenLantern*. scale bar 10µm.

1547 **Movie S6**: Maximum intensity projection of LightSheet Z-stack live imaging of *scFv-*
1548 *mAvic1* embryo. Upper part: dorsal view, lower part: ventral view Scale bar 100µm.

1549 **Movie S7**: Maximum intensity projection of LightSheet Z-stack live imaging of *scFv-*
1550 *msGFP2* embryo. Upper part: dorsal view, lower part: ventral view Scale bar 100µm.

1551 **Movie S8**: Maximum intensity projection of confocal Z-stack fast live imaging of an
1552 embryo containing *scFv-NeonGreen>twi_suntag_MS2_CRISPR/+.* Translation foci
1553 are in green, scale bar 1μm.
1554 **Movie S9**: Maximum intensity projection of confocal Z-stack fast live imaging of an
1555 embryo containing *scFv-sfGFP >twi_suntag_MS2_CRISPR/+.* Translation foci are in
1556 green, scale bar 1μm.
1557 **Movie S10**: Maximum intensity projection of confocal Z-stack fast live imaging of an
1558 embryo containing *scFv-GreenLantern >twi_suntag_MS2_CRISPR/+.* Translation foci
1559 are in green, scale bar 1μm.
1560 **Movie S11**: Maximum intensity projection of confocal Z-stack fast live imaging of an
1561 embryo containing *scFv-msGFP2>twi_suntag_MS2_CRISPR/+.* Translation foci are in
1562 green, scale bar 1μm.
1563 **Movie S12**: Maximum intensity projection of confocal Z-stack fast live imaging of an
1564 embryo containing *scFv-mAvic1>twi_suntag_MS2_CRISPR/+.* Translation foci are in
1565 green, scale bar 1μm.
1566 **Movie S13**: Maximum intensity projection of confocal Z-stack live imaging of an
1567 embryo containing *scFv-msGFP2>twi_suntag_MS2_CRISPR/+.* Translation foci are in
1568 white, scale bar 10μm.
1569 **Movie S14**: Maximum intensity projection of confocal Z-stack live imaging of an
1570 embryo containing *scFv-msGFP2>twi_suntag_transgene/+.* Translation foci are in
1571 white, scale bar 10μm.
1572 **Movie S15**: Maximum intensity projection of confocal Z-stack live imaging of an
1573 embryo containing *scFv-mAvic1> twi_suntag_transgene/+.* Translation foci are in
1574 white, scale bar 10μm.

1575 **Movie S16**: Maximum intensity projection of confocal Z-stack live imaging of an
1576 embryo containing *nos-Gal4>UASp-scFv-GreenLantern /*+. scale bar 10µm.
1577 **Movie S17**: Maximum intensity projection of confocal Z-stack live imaging of an
1578 embryo containing *nos-Gal4>UASp-scFv-msGFP2 /*+. scale bar 10µm.
1579 **Movie S18**: Maximum intensity projection of confocal Z-stack live imaging of an
1580 embryo containing *nos-Gal4>UASp-scFv-NeonGreen /*+. scale bar 10µm.
1581 **Movie S19**: Maximum intensity projection of confocal Z-stack live imaging of an
1582 embryo containing *nos-Gal4>UASp-scFv-mAvic1 /*+. scale bar 10µm.
1583 **Movie S20**: Comparison of maximum intensity projection of confocal Z-stack live
1584 imaging of an embryo containing *scFv-msGFP2>twi_suntag_MS2_CRISPR/*+ *or nos-*
1585 *Gal4>UASp-scFv-mAvic1 ; twi_suntag_MS2_CRISPR/*+. Translation foci are in white.
1586 Translationnal arrest is seen *scFv-msGFP2>twi_suntag_MS2_CRISPR/*+ *but not* in
1587 *nos-Gal4>UASp-scFv-mAvic1 ; twi_suntag_MS2_CRISPR/*+. scale bar 10µm.
1588 **Movie S21**: Maximum intensity projection of confocal Z-stack live imaging of an
1589 embryo containing *nos-Gal4>UASy-scFv-msGFP2 /*+. scale bar 10µm.
1590 **Movie S22**: Maximum intensity projection of confocal Z-stack live imaging of an
1591 embryo containing *nullo-Gal4>UASy-scFv-msGFP2 /*+. scale bar 100µm.
1592 **Movie S23**: Maximum intensity projection of confocal Z-stack live imaging of an
1593 embryo containing *NB-ALFA-msGFP2*. scale bar 10µm.
1594 **Movie S24**: Maximum intensity projection of confocal Z-stack live imaging of an
1595 embryo containing *NB-ALFA-msGFP2> Ilp4_32x_ALFA-array/*+. Scale bar 10µm.
1596 **Movie S25**: Maximum intensity projection of confocal tile-scan with Z-stack live
1597 imaging of an embryo containing *NB-ALFA-msGFP2> Ilp4_32x_ALFA-array/*+. Scale
1598 bar 100µm.

1599 **Movie S26**: Single plane of a confocal live imaging of an embryo containing
1600 *twi_suntag_MS2_CRISPR/+; NB-ALFA_msGFP2/scFv-mScarlet x Ilp4_32x_ALFA-*
1601 *array* during n.c.14. Scale bar 5µm.
1602 **Movie S27**: Single plane of a confocal live imaging of an embryo containing *NB-*
1603 *ALFA_msGFP2/scFv-mScarlet x Ilp4_32x_ALFA-array* during n.c.14. Scale bar 5µm.
1604

Figure 1

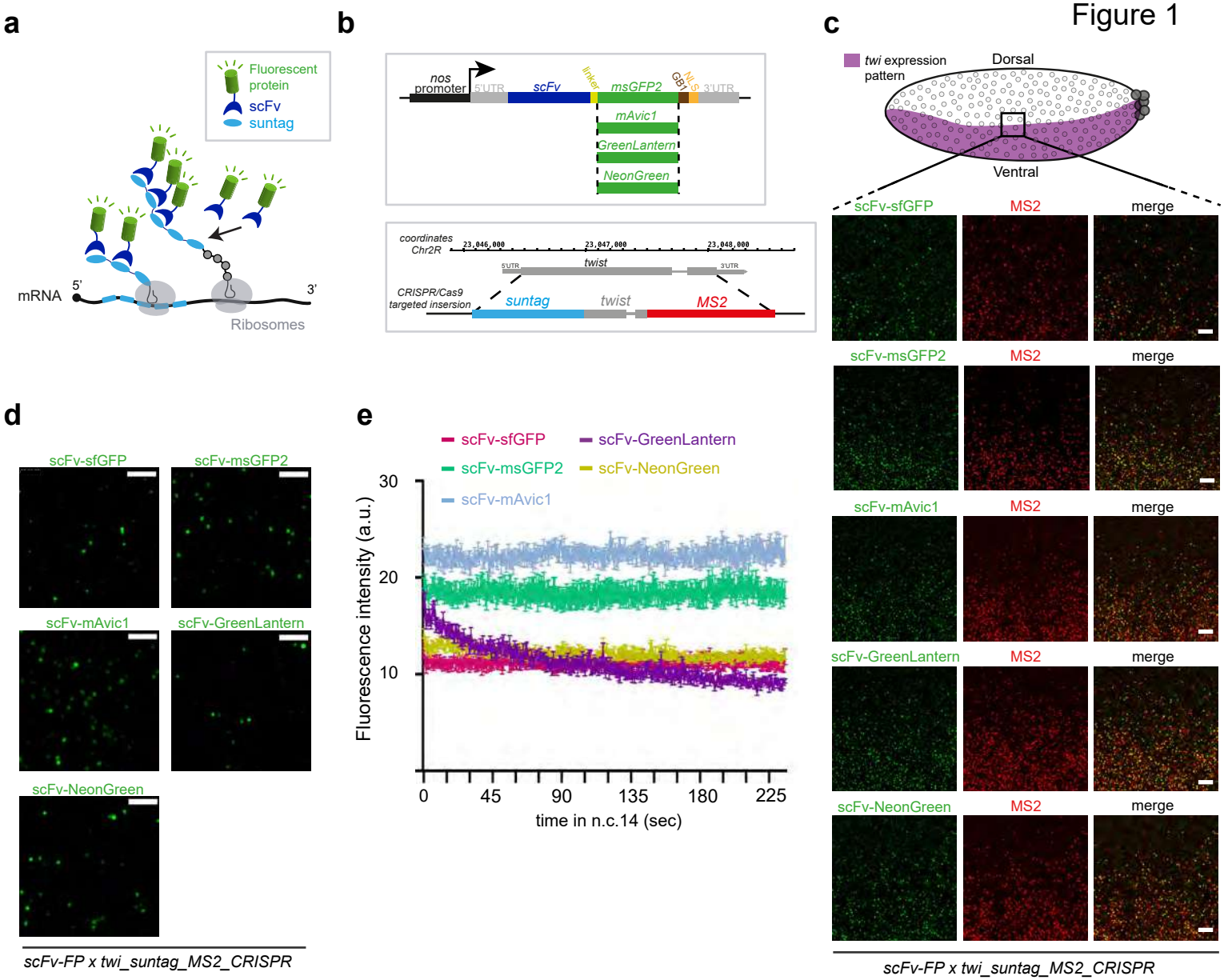
a
Fluorescent protein
scFv
suntag
mRNA
5'
3'
Ribosomes
b
nos promoter
5'UTR
scFv
linker
msGFP2
GBM
NLS
3'UTR
mAvic1
GreenLantern
NeonGreen
coordinates Chr2R
23,046,000
23,047,000
23,048,000
5'UTR
twist
3'UTR
CRISPR/Cas9 targeted insersion
suntag
twist
MS2
c
twi expression pattern
Dorsal
Ventral
scFv-sfGFP
MS2
merge
scFv-msGFP2
MS2
merge
scFv-mAvic1
MS2
merge
scFv-GreenLantern
MS2
merge
scFv-NeonGreen
MS2
merge
scFv-FP x twi_suntag_MS2_CRISPR
d
scFv-sfGFP
scFv-msGFP2
scFv-mAvic1
scFv-GreenLantern
scFv-NeonGreen
scFv-FP x twi_suntag_MS2_CRISPR
e
scFv-sfGFP
scFv-GreenLantern
scFv-msGFP2
scFv-NeonGreen
scFv-mAvic1
Fluorescence intensity (a.u.)
30
20
10
0
45
90
135
180
225
time in n.c.14 (sec)

Figure 2

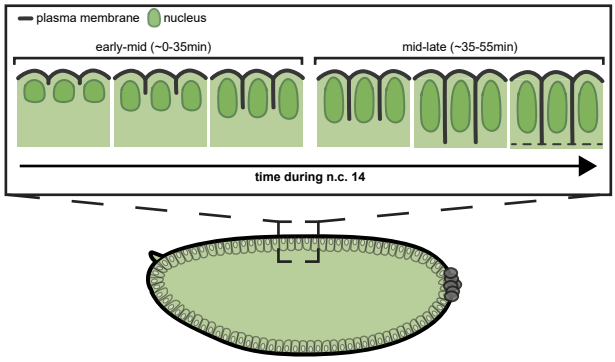
a
plasma membrane
nucleus
early-mid (~0-35min)
mid-late (~35-55min)
time during n.c. 14

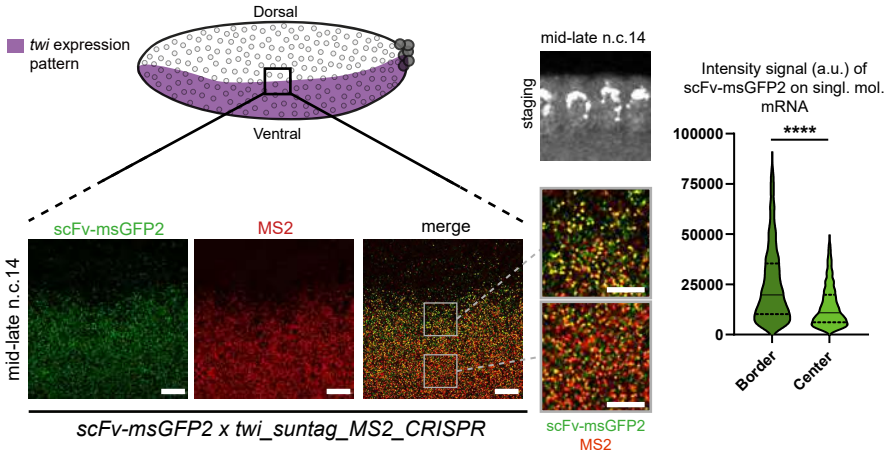
b
twi expression pattern
Dorsal
Ventral
mid-late n.c.14
staging
scFv-msGFP2
MS2
merge
mid-late n.c.14
scFv-msGFP2 x twi_suntag_MS2_CRISPR
scFv-msGFP2
MS2
Intensity signal (a.u.) of scFv-msGFP2 on singl. mol. mRNA
****
100000
75000
50000
25000
0
Border
Center

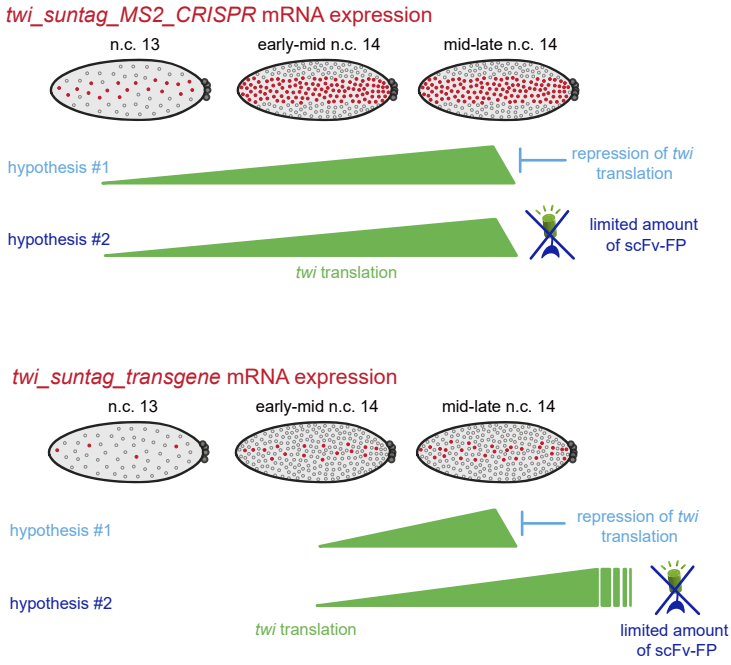
c
twi_suntag_MS2_CRISPR mRNA expression
n.c. 13
early-mid n.c. 14
mid-late n.c. 14
hypothesis #1
repression of twi translation
hypothesis #2
limited amount of scFv-FP
twi translation
twi_suntag_transgene mRNA expression
n.c. 13
early-mid n.c. 14
mid-late n.c. 14
hypothesis #1
repression of twi translation
hypothesis #2
twi translation
limited amount of scFv-FP

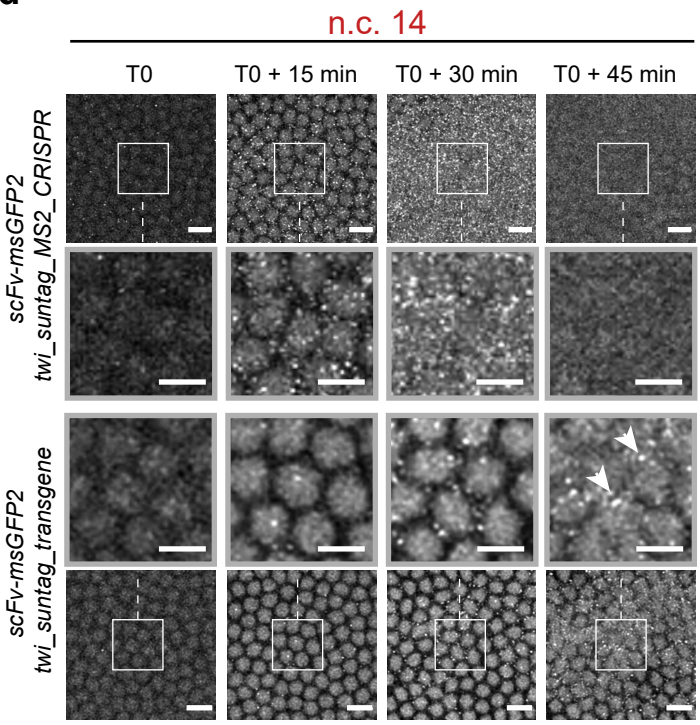
d
n.c. 14
T0
T0 + 15 min
T0 + 30 min
T0 + 45 min
scFv-msGFP2 twi_suntag_MS2_CRISPR
scFv-msGFP2 twi_suntag_transgene

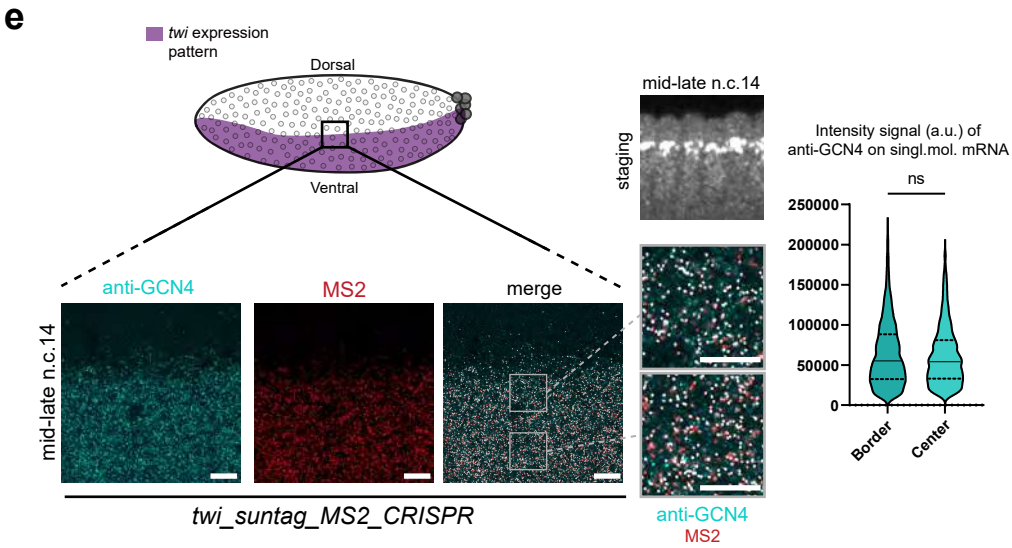
e
twi expression pattern
Dorsal
Ventral
mid-late n.c.14
staging
anti-GCN4
MS2
merge
mid-late n.c.14
twi_suntag_MS2_CRISPR
anti-GCN4
MS2
Intensity signal (a.u.) of anti-GCN4 on singl.mol. mRNA
ns
250000
200000
150000
100000
50000
0
Border
Center

Figure 3

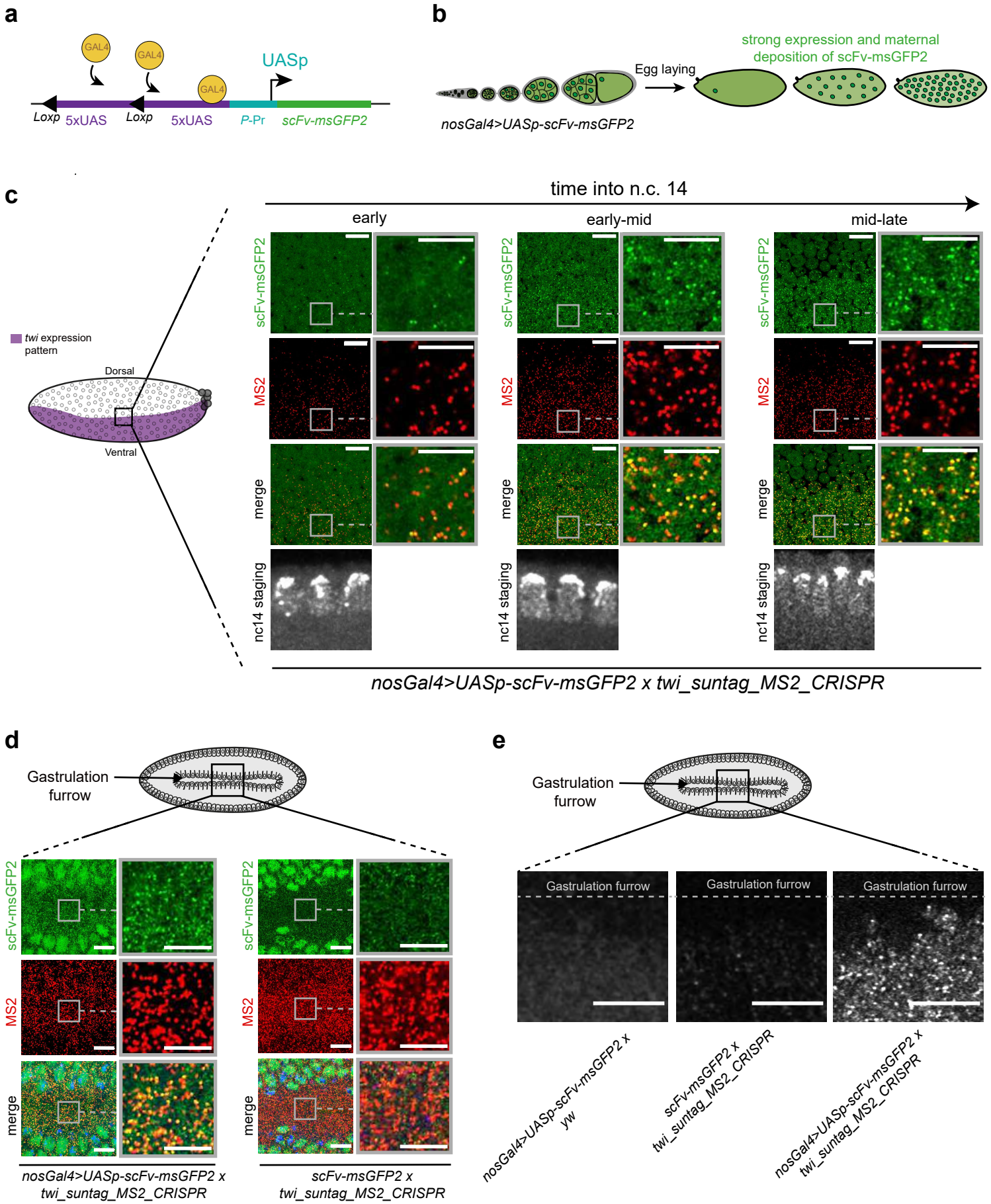
a
GAL4
GAL4
GAL4
UASp
Loxp
5xUAS
Loxp
5xUAS
P-Pr
scFv-msGFP2
b
strong expression and maternal deposition of scFv-msGFP2
Egg laying
nosGal4>UASp-scFv-msGFP2
c
time into n.c. 14
early
early-mid
mid-late
twi expression pattern
Dorsal
Ventral
scFv-msGFP2
MS2
merge
nc14 staging
nosGal4>UASp-scFv-msGFP2 x twi_suntag_MS2_CRISPR
d
Gastrulation furrow
scFv-msGFP2
MS2
merge
nosGal4>UASp-scFv-msGFP2 x twi_suntag_MS2_CRISPR
scFv-msGFP2 x twi_suntag_MS2_CRISPR
e
Gastrulation furrow
Gastrulation furrow
Gastrulation furrow
Gastrulation furrow
nosGal4>UASp-scFv-msGFP2 x yw
scFv-msGFP2 x twi_suntag_MS2_CRISPR
nosGal4>UASp-scFv-msGFP2 x twi_suntag_MS2_CRISPR

Figure 4

**a**

**suntag V4 sequence (19aa) and linker (5aa):**
**EELLSKNYHLENEVARLKK GSGSG**

**ALFA-tag V1 sequence (15aa) and linker (5aa):**
**PSRLEEELRRRLTEP GSGSG**

**b**

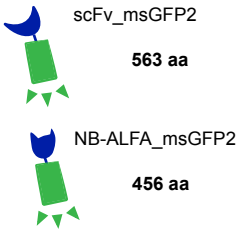


**c**

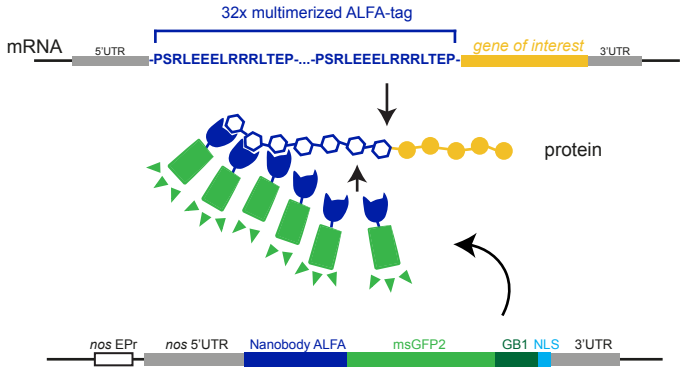


**d**

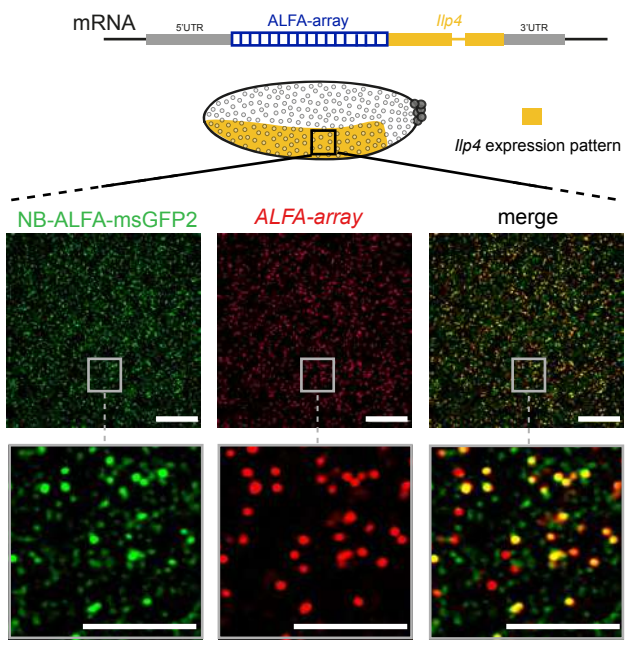


*NB-ALFA-msGFP2 x llp4_32x_ALFA-array*

**e**

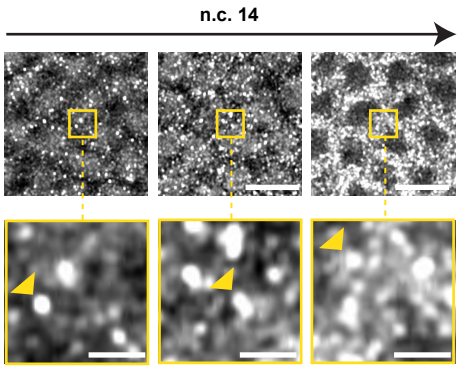


*NB-ALFA-msGFP2 x llp4_32x_ALFA-array*

**f**

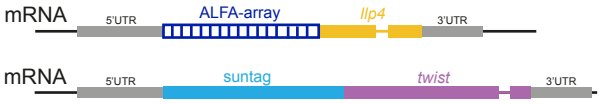


**g**

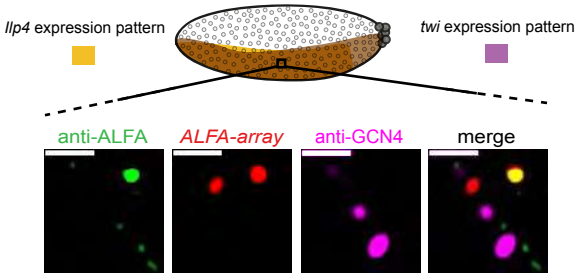


*llp4_32x_ALFA-array ; twi_suntag_transgene*

**h**

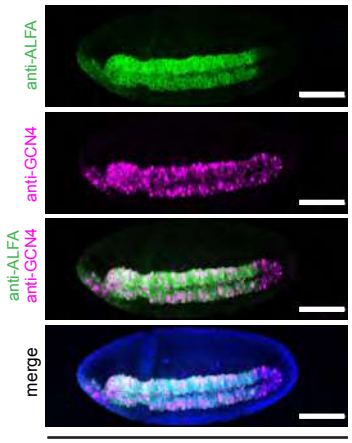


*llp4_32x_ALFA-array ; twi_suntag_transgene*

**i**

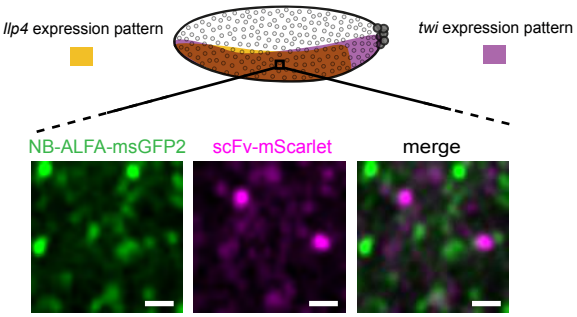


*twi_suntag_MS2_CRISPR/+;NB-ALFA-msGFP2/ scFv-mScarlet x llp4_32x_ALFA-array*

**j**

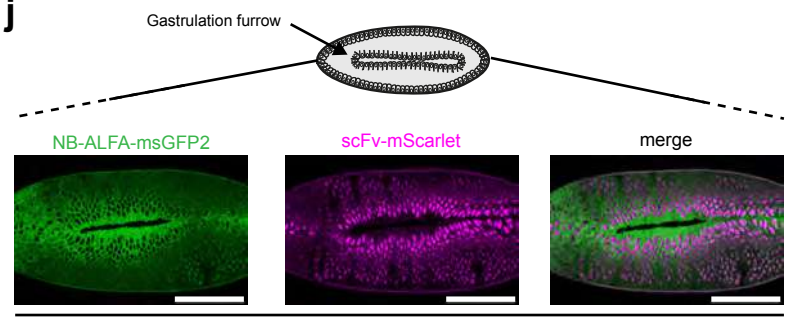


*twi_suntag_MS2_CRISPR/+;NB-ALFA-msGFP2/scFv-mScarlet x llp4_32x_ALFA-array*

Figure 5

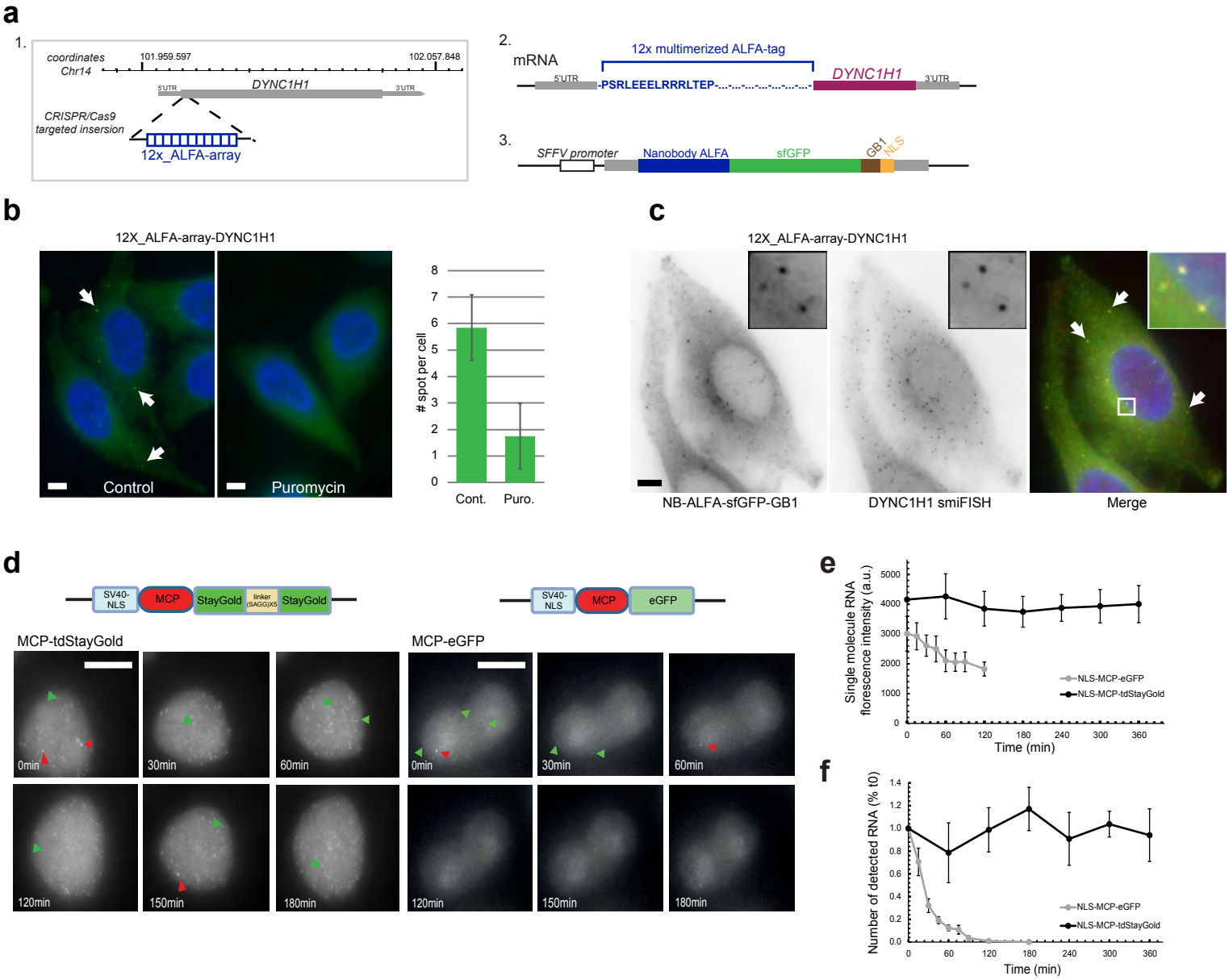
a
1.
coordinates
Chr14
101.959.597
102.057.848
5'UTR
DYNC1H1
3'UTR
CRISPR/Cas9
targeted insersion
12x_ALFA-array
2.
mRNA
12x multimerized ALFA-tag
5'UTR
-PSRLEEELRRRLTEP-...-...-...-...-...-...-
DYNC1H1
3'UTR
3.
SFFV promoter
Nanobody ALFA
sfGFP
GB1
NLS
b
12X_ALFA-array-DYNC1H1
Control
Puromycin
# spot per cell
Cont.
Puro.
c
12X_ALFA-array-DYNC1H1
NB-ALFA-sfGFP-GB1
DYNC1H1 smiFISH
Merge
d
SV40-NLS
MCP
StayGold
linker (SAGG)X5
StayGold
SV40-NLS
MCP
eGFP
MCP-tdStayGold
MCP-eGFP
0min
30min
60min
120min
150min
180min
e
Single molecule RNA florescence intensity (a.u.)
Time (min)
NLS-MCP-eGFP
NLS-MCP-tdStayGold
f
Number of detected RNA (% t0)
Time (min)
NLS-MCP-eGFP
NLS-MCP-tdStayGold

Figure S1

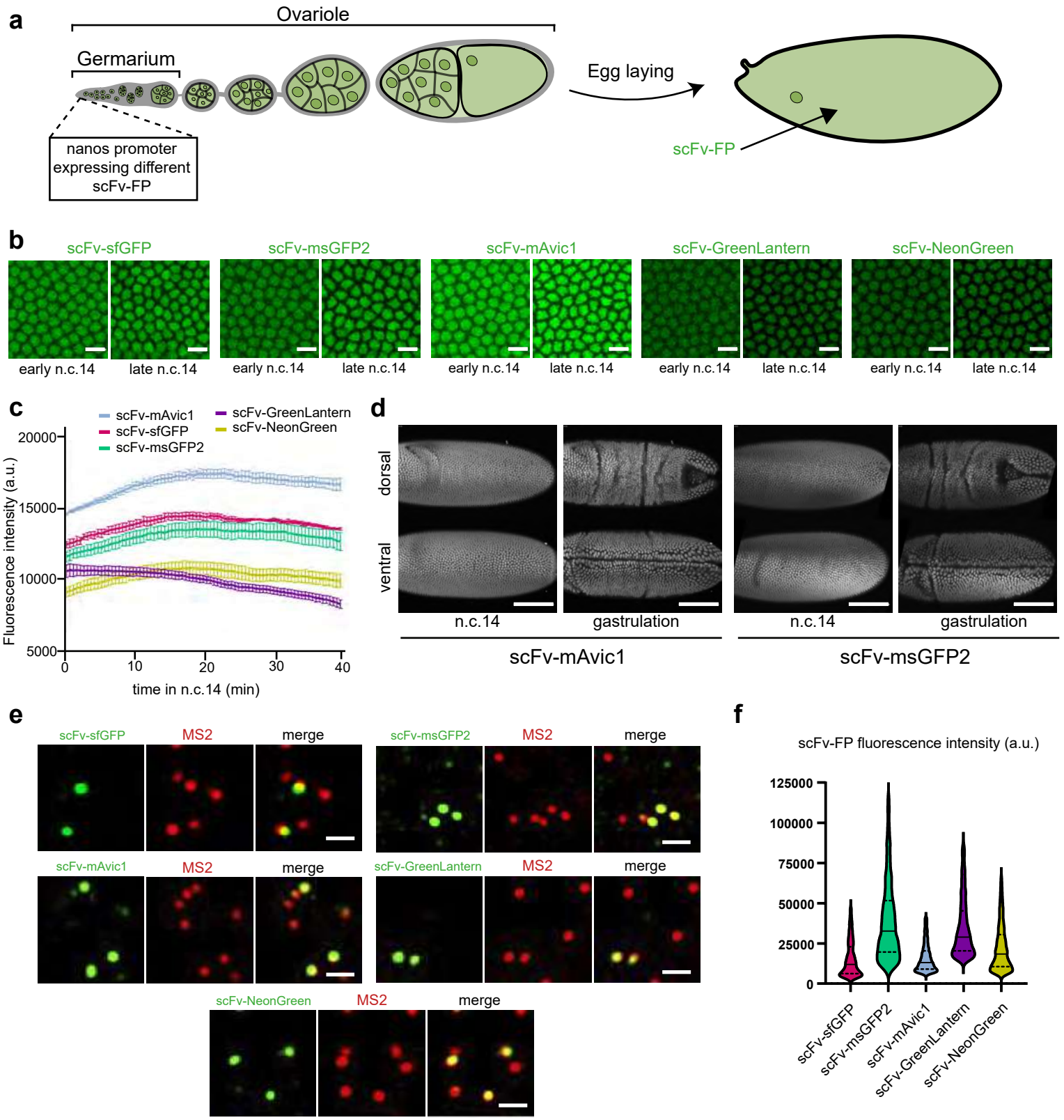
a
Ovariole
Germarium
nanos promoter expressing different scFv-FP
Egg laying
scFv-FP
b
scFv-sfGFP
scFv-msGFP2
scFv-mAvic1
scFv-GreenLantern
scFv-NeonGreen
early n.c.14
late n.c.14
c
scFv-mAvic1
scFv-sfGFP
scFv-msGFP2
scFv-GreenLantern
scFv-NeonGreen
Fluorescence intensity (a.u.)
20000
15000
10000
5000
0
10
20
30
40
time in n.c.14 (min)
d
dorsal
ventral
n.c.14
gastrulation
scFv-mAvic1
scFv-msGFP2
e
scFv-sfGFP
MS2
merge
scFv-msGFP2
scFv-mAvic1
scFv-GreenLantern
scFv-NeonGreen
f
scFv-FP fluorescence intensity (a.u.)
125000
100000
75000
50000
25000
0
scFv-sfGFP
scFv-msGFP2
scFv-mAvic1
scFv-GreenLantern
scFv-NeonGreen

Figure S2

**a**

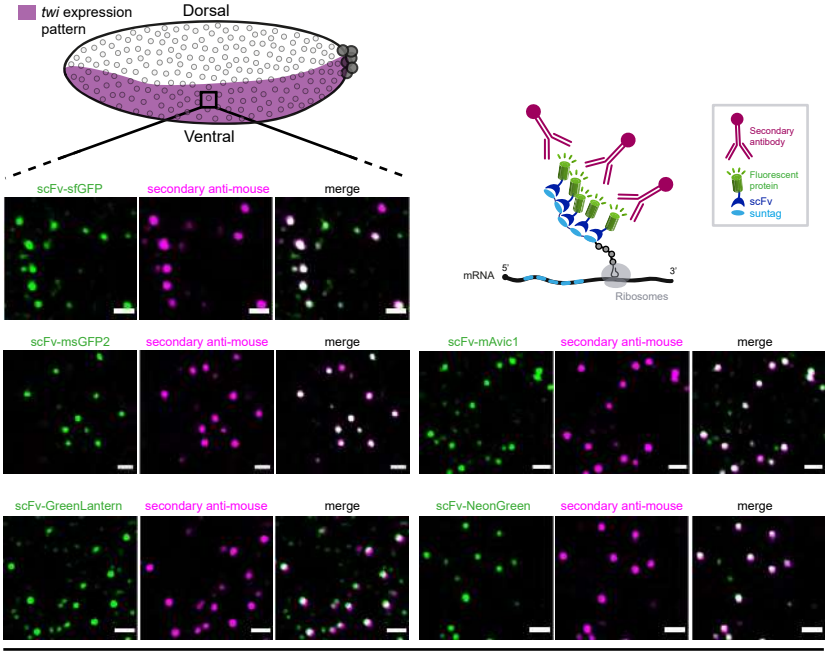


*scFv-FP x twi_suntag_MS2_CRISPR*

**b**

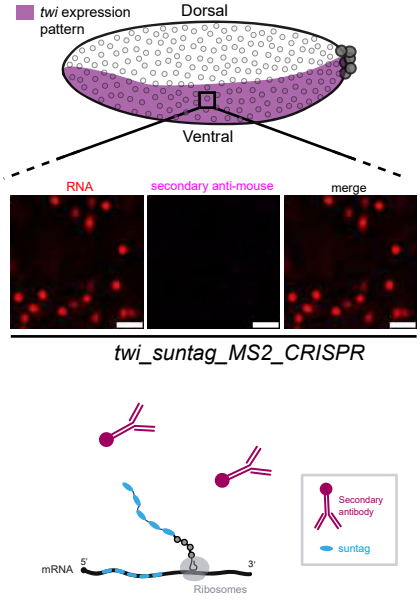


*twi_suntag_MS2_CRISPR*

**c**

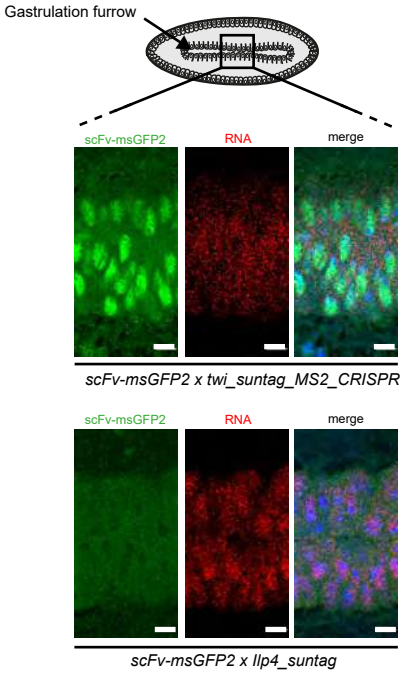


*scFv-msGFP2 x twi_suntag_MS2_CRISPR*

*scFv-msGFP2 x llp4_suntag*

Figure S3

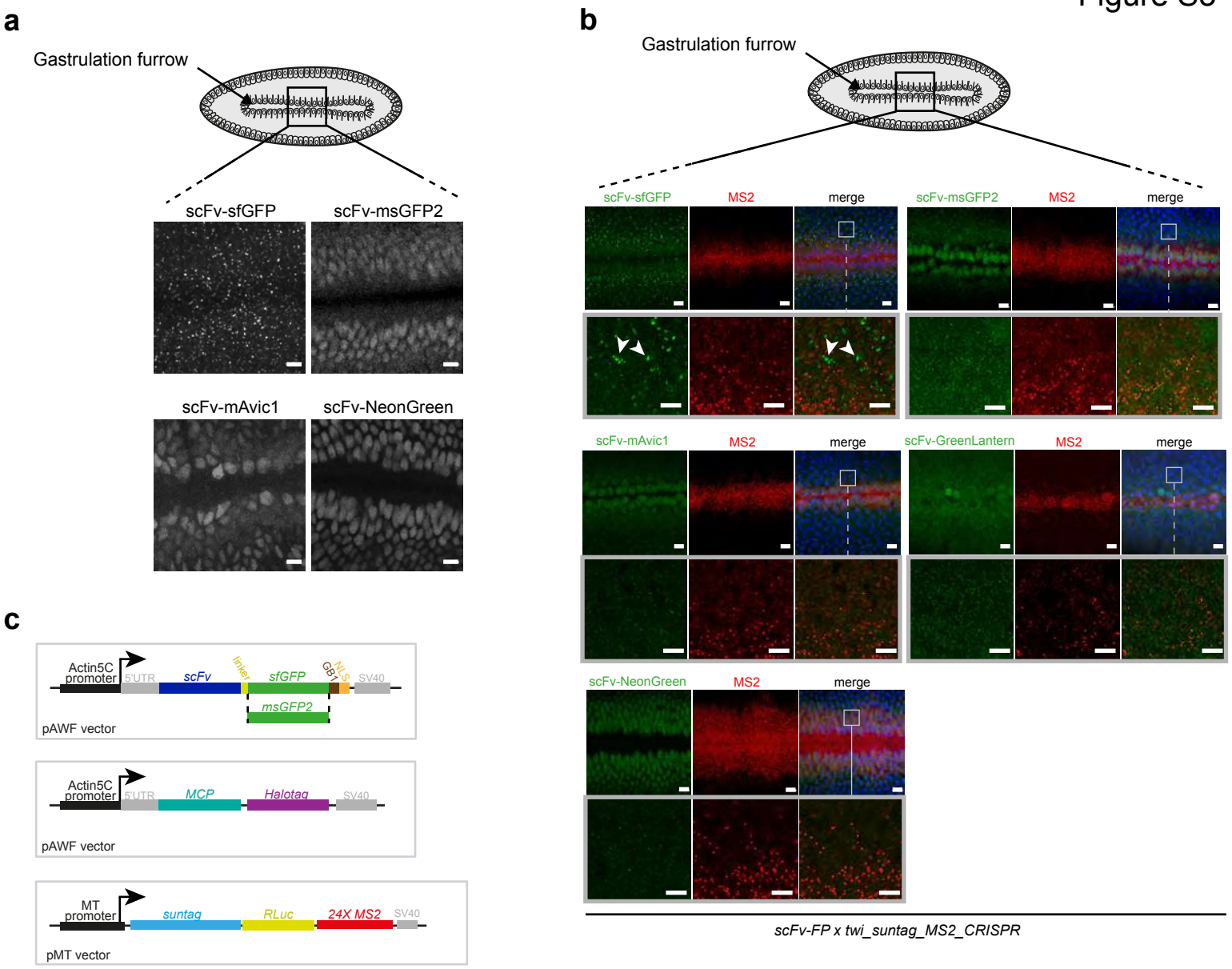
a
Gastrulation furrow
scFv-sfGFP
scFv-msGFP2
scFv-mAvic1
scFv-NeonGreen
b
Gastrulation furrow
scFv-sfGFP
MS2
merge
scFv-msGFP2
MS2
merge
scFv-mAvic1
MS2
merge
scFv-GreenLantern
MS2
merge
scFv-NeonGreen
MS2
merge
scFv-FP x twi_suntag_MS2_CRISPR
c
Actin5C promoter
5'UTR
scFv
linker
sfGFP
GB
N.S
SV40
msGFP2
pAWF vector
Actin5C promoter
5'UTR
MCP
Halotag
SV40
pAWF vector
MT promoter
suntag
RLuc
24X MS2
SV40
pMT vector

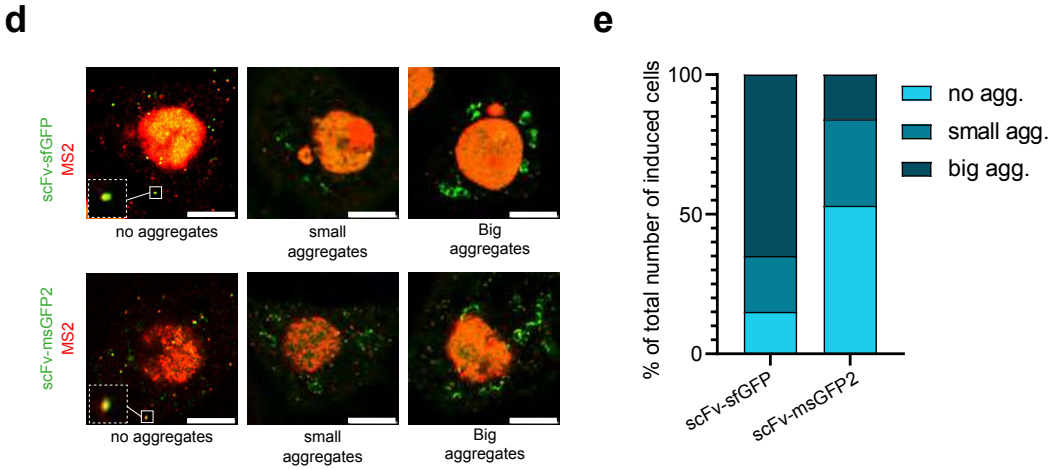
d
scFv-sfGFP
MS2
no aggregates
small aggregates
Big aggregates
scFv-msGFP2
MS2
no aggregates
small aggregates
Big aggregates
e
% of total number of induced cells
100
50
0
scFv-sfGFP
scFv-msGFP2
no agg.
small agg.
big agg.

Figure S4

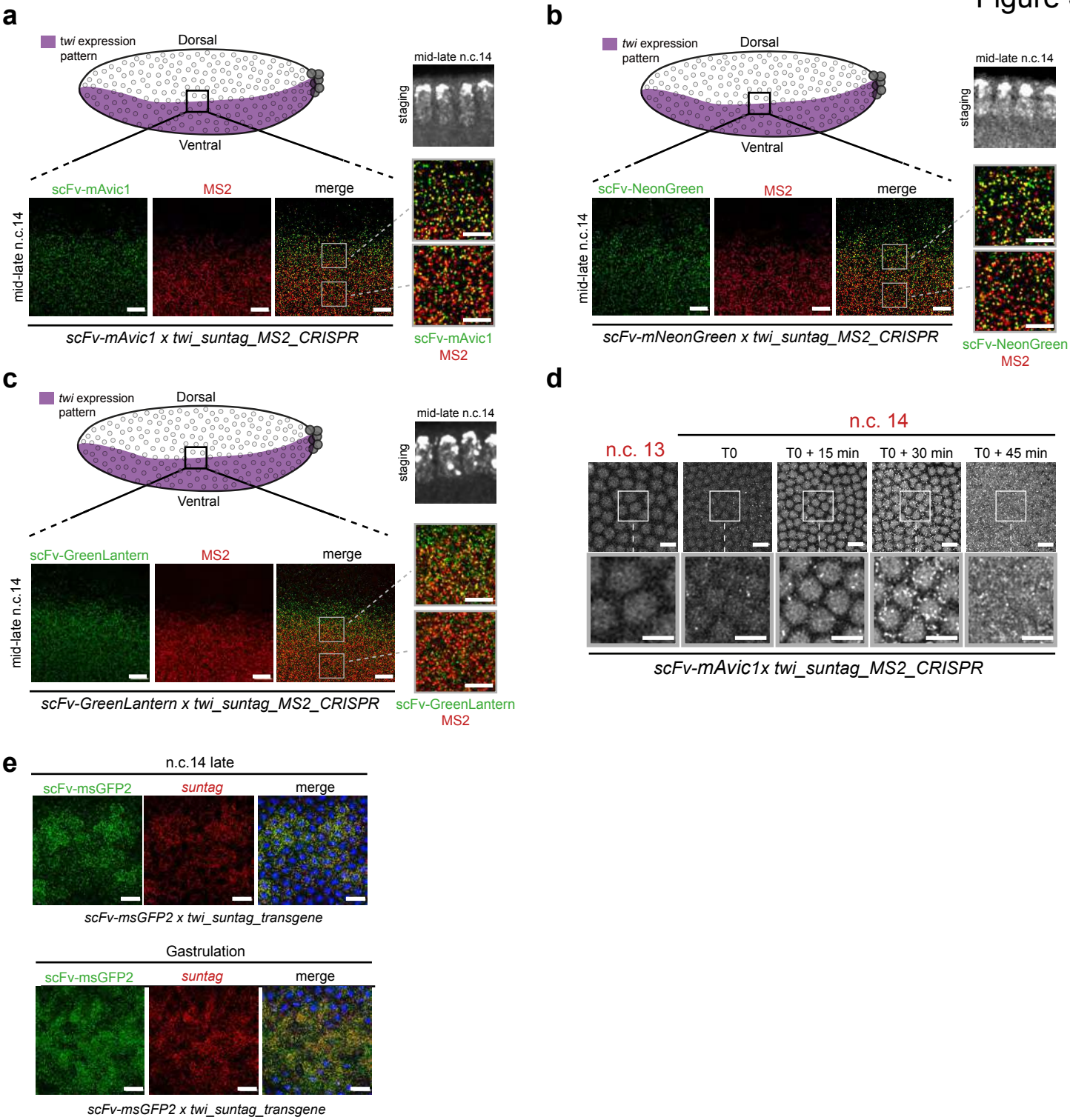
a
twi expression pattern
Dorsal
Ventral
mid-late n.c.14
staging
scFv-mAvic1
MS2
merge
mid-late n.c.14
scFv-mAvic1 x twi_suntag_MS2_CRISPR
scFv-mAvic1
MS2
b
twi expression pattern
Dorsal
Ventral
mid-late n.c.14
staging
scFv-NeonGreen
MS2
merge
mid-late n.c.14
scFv-mNeonGreen x twi_suntag_MS2_CRISPR
scFv-NeonGreen
MS2
c
twi expression pattern
Dorsal
Ventral
mid-late n.c.14
staging
scFv-GreenLantern
MS2
merge
mid-late n.c.14
scFv-GreenLantern x twi_suntag_MS2_CRISPR
scFv-GreenLantern
MS2
d
n.c. 14
n.c. 13
T0
T0 + 15 min
T0 + 30 min
T0 + 45 min
scFv-mAvic1x twi_suntag_MS2_CRISPR
e
n.c.14 late
scFv-msGFP2
suntag
merge
scFv-msGFP2 x twi_suntag_transgene
Gastrulation
scFv-msGFP2
suntag
merge
scFv-msGFP2 x twi_suntag_transgene

Figure S5

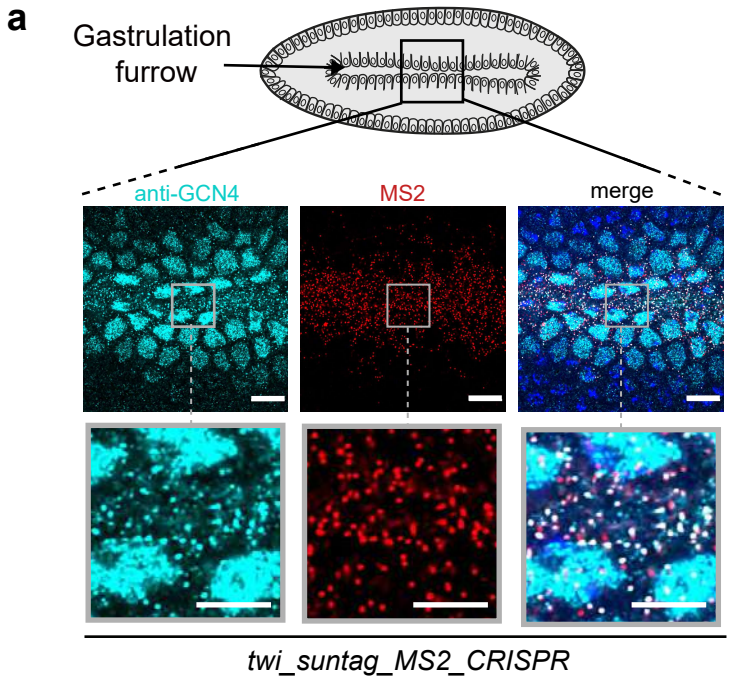
a
Gastrulation furrow
anti-GCN4
MS2
merge
twi_suntag_MS2_CRISPR

Figure S6

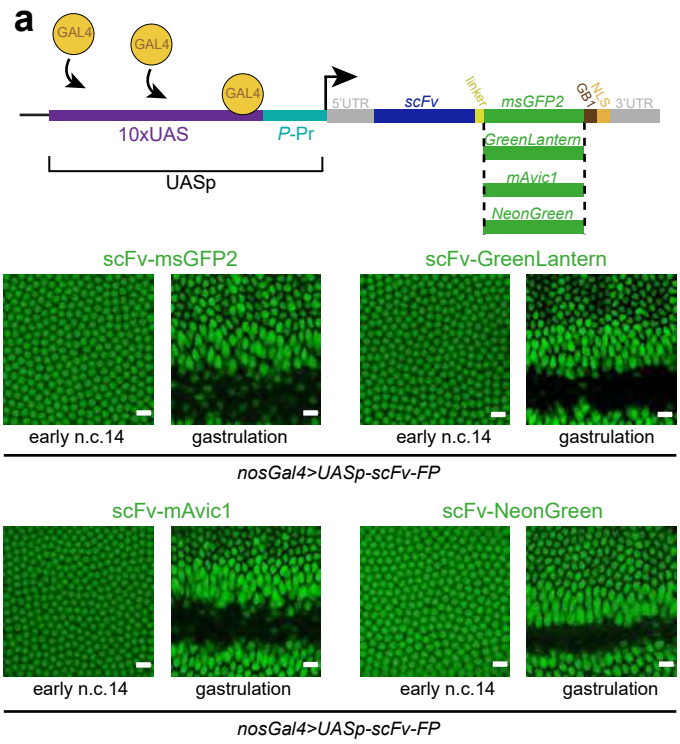
a
GAL4
GAL4
GAL4
10xUAS
P-Pr
UASp
5'UTR
scFv
linker
msGFP2
GB1
NLS
3'UTR
GreenLantern
mAvic1
NeonGreen
scFv-msGFP2
scFv-GreenLantern
early n.c.14
gastrulation
early n.c.14
gastrulation
nosGal4>UASp-scFv-FP
scFv-mAvic1
scFv-NeonGreen
early n.c.14
gastrulation
early n.c.14
gastrulation
nosGal4>UASp-scFv-FP

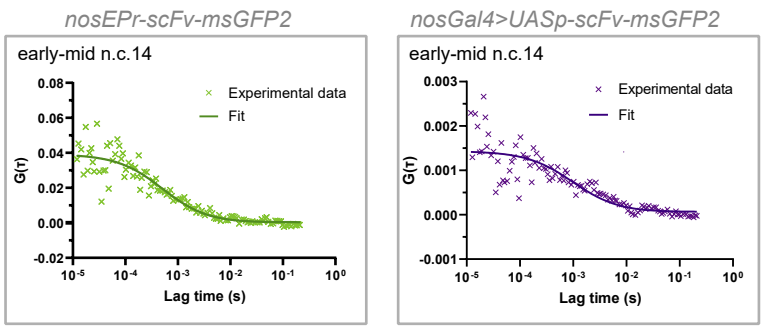
b
nosEPr-scFv-msGFP2
nosGal4>UASp-scFv-msGFP2
early-mid n.c.14
Experimental data
Fit
G(τ)
Lag time (s)
early-mid n.c.14
Experimental data
Fit
G(τ)
Lag time (s)

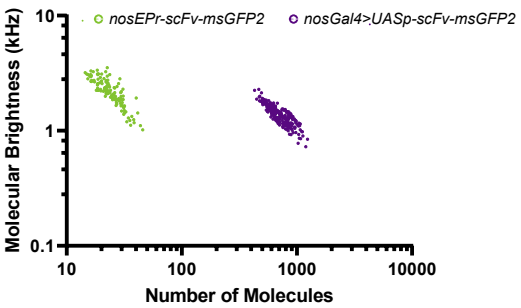
c
nosEPr-scFv-msGFP2
nosGal4>UASp-scFv-msGFP2
Molecular Brightness (kHz)
Number of Molecules

Figure S7

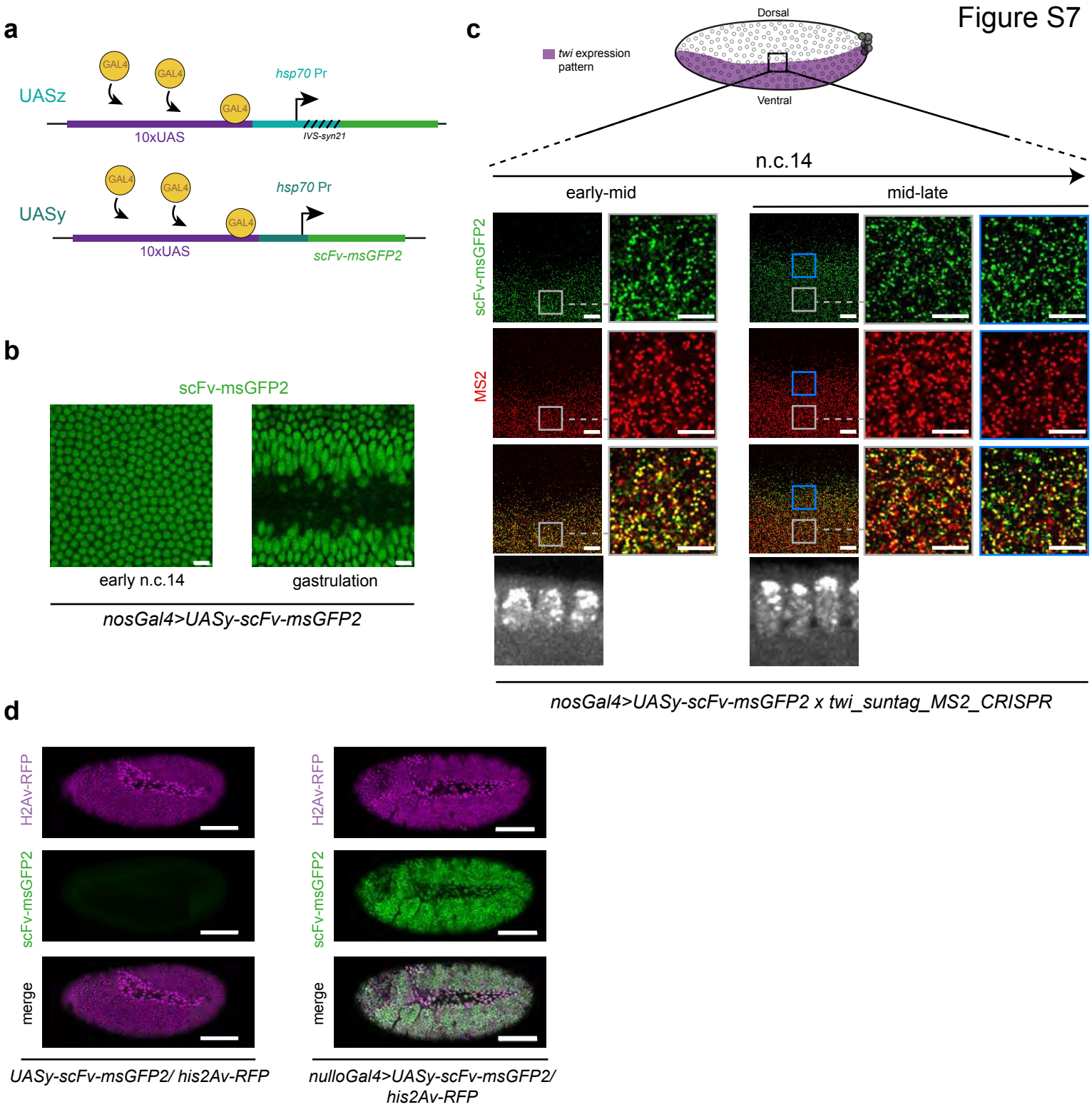
a
UASz
GAL4
GAL4
GAL4
hsp70 Pr
10xUAS
IVS-syn21
UASy
GAL4
GAL4
GAL4
hsp70 Pr
10xUAS
scFv-msGFP2
b
scFv-msGFP2
early n.c.14
gastrulation
nosGal4>UASy-scFv-msGFP2
c
Dorsal
twi expression pattern
Ventral
n.c.14
early-mid
mid-late
scFv-msGFP2
MS2
nosGal4>UASy-scFv-msGFP2 x twi_suntag_MS2_CRISPR
d
H2Av-RFP
scFv-msGFP2
merge
UASy-scFv-msGFP2/ his2Av-RFP
nulloGal4>UASy-scFv-msGFP2/ his2Av-RFP

Figure S8

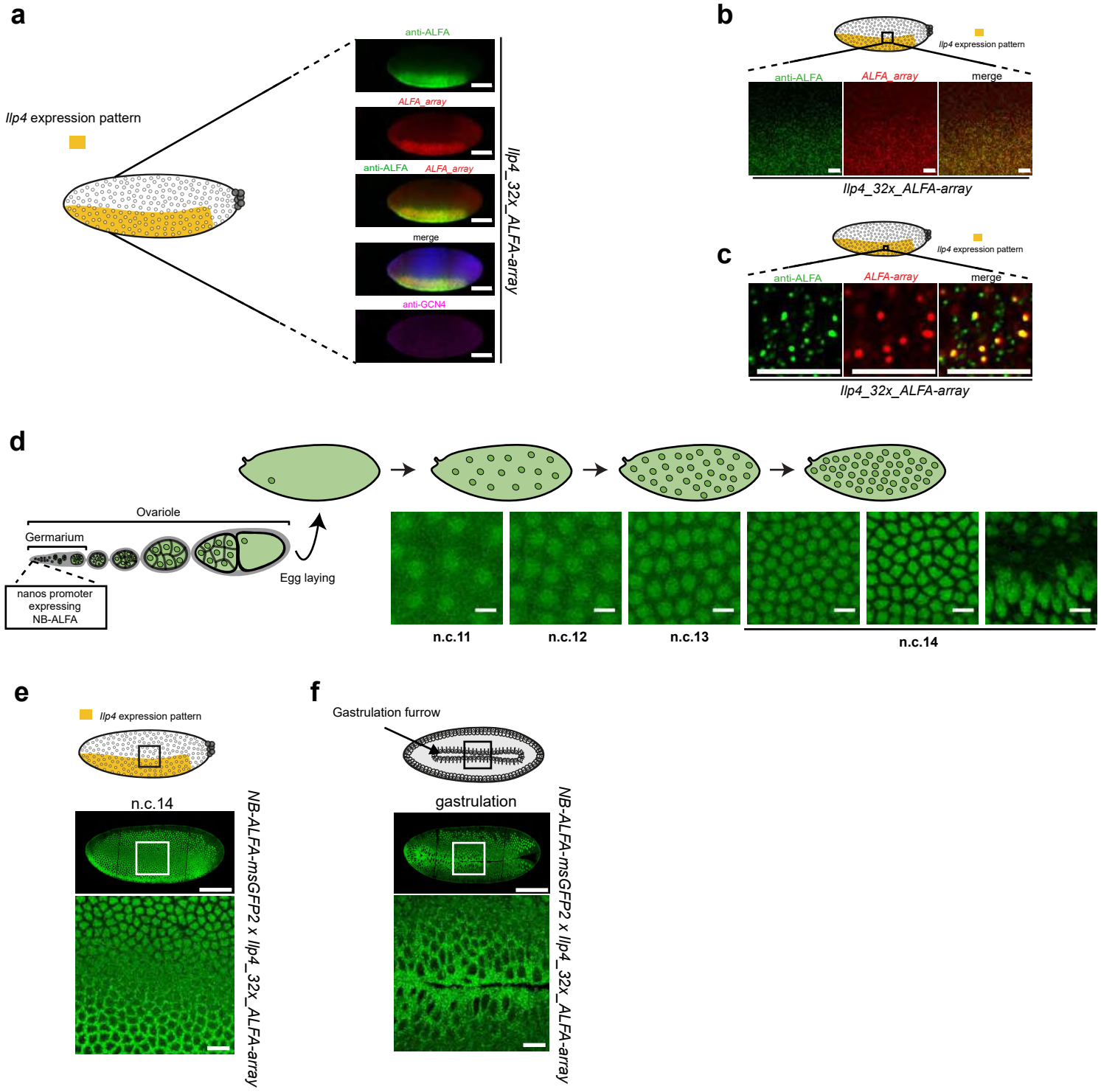
a
llp4 expression pattern
anti-ALFA
ALFA_array
anti-ALFA ALFA_array
merge
anti-GCN4
llp4_32x_ALFA-array
b
llp4 expression pattern
anti-ALFA
ALFA_array
merge
llp4_32x_ALFA-array
c
llp4 expression pattern
anti-ALFA
ALFA-array
merge
llp4_32x_ALFA-array
d
Ovariole
Germarium
nanos promoter expressing NB-ALFA
Egg laying
n.c.11
n.c.12
n.c.13
n.c.14
e
llp4 expression pattern
n.c.14
NB-ALFA-msGFP2 x llp4_32x_ALFA-array
f
Gastrulation furrow
gastrulation
NB-ALFA-msGFP2 x llp4_32x_ALFA-array

Figure S9

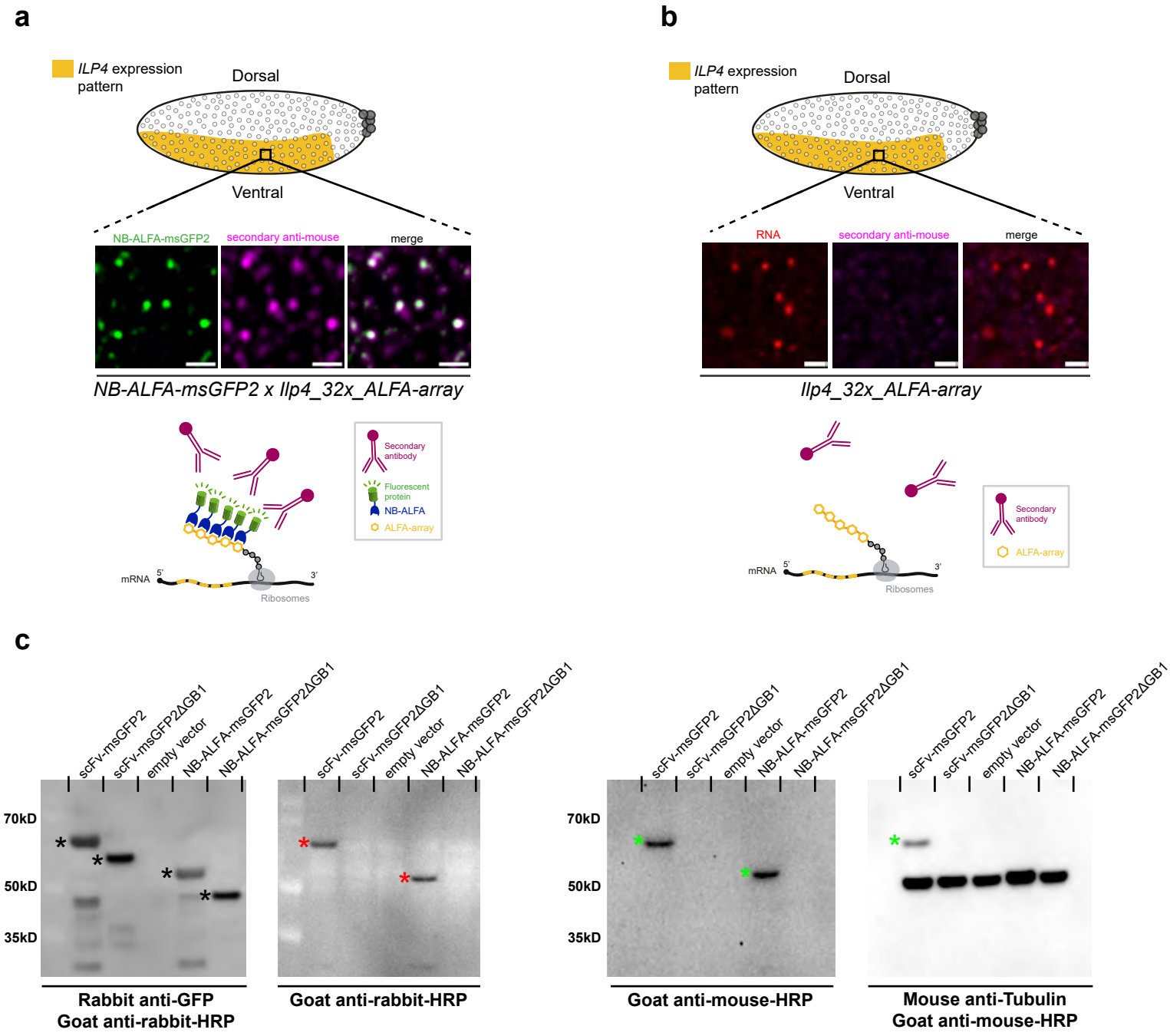
a
ILP4 expression pattern
Dorsal
Ventral
NB-ALFA-msGFP2
secondary anti-mouse
merge
NB-ALFA-msGFP2 x Ilp4_32x_ALFA-array
Secondary antibody
Fluorescent protein
NB-ALFA
ALFA-array
mRNA
5'
3'
Ribosomes
b
ILP4 expression pattern
Dorsal
Ventral
RNA
secondary anti-mouse
merge
Ilp4_32x_ALFA-array
Secondary antibody
ALFA-array
mRNA
5'
3'
Ribosomes
c
scFv-msGFP2
scFv-msGFP2ΔGB1
empty vector
NB-ALFA-msGFP2
NB-ALFA-msGFP2ΔGB1
70kD
50kD
35kD
Rabbit anti-GFP
Goat anti-rabbit-HRP
Goat anti-rabbit-HRP
Goat anti-mouse-HRP
Mouse anti-Tubulin
Goat anti-mouse-HRP

Figure S10

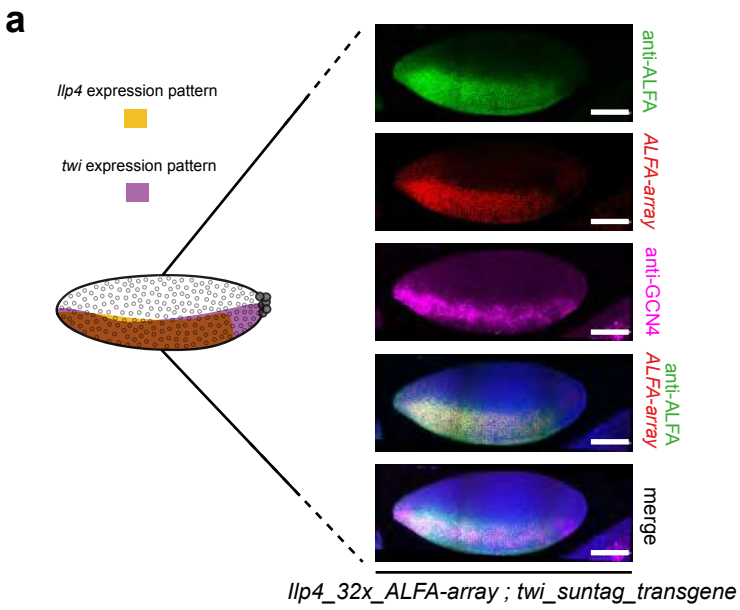
a
*llp4* expression pattern
*twi* expression pattern
anti-ALFA
*ALFA-array*
anti-GCN4
anti-ALFA
*ALFA-array*
merge
*llp4_32x_ALFA-array ; twi_suntag_transgene*

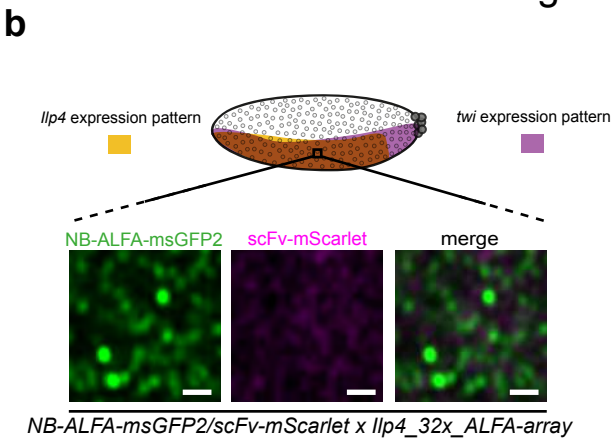
b
*llp4* expression pattern
*twi* expression pattern
NB-ALFA-msGFP2
scFv-mScarlet
merge
*NB-ALFA-msGFP2/scFv-mScarlet x llp4_32x_ALFA-array*

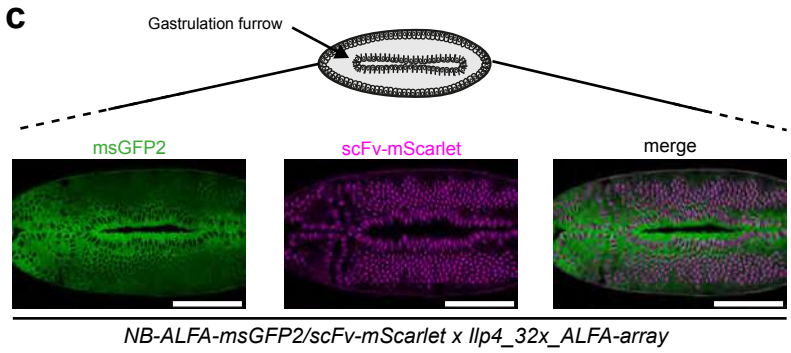
c
Gastrulation furrow
msGFP2
scFv-mScarlet
merge
*NB-ALFA-msGFP2/scFv-mScarlet x llp4_32x_ALFA-array*

Figure S11

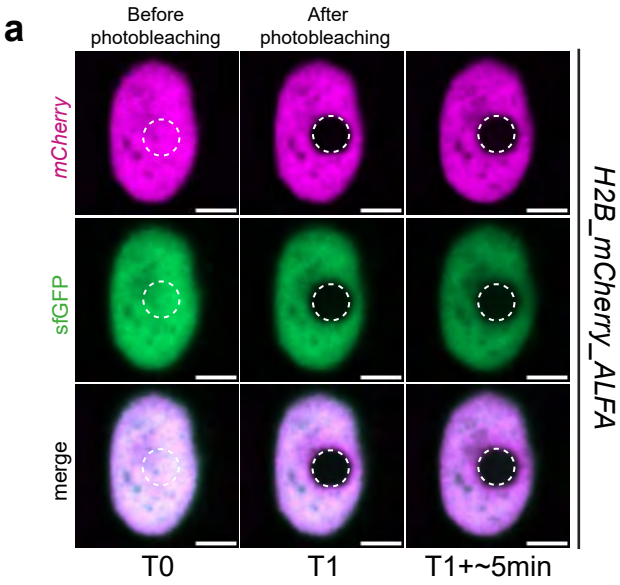
a
Before photobleaching
After photobleaching
mCherry
sfGFP
merge
H2B_mCherry_ALFA
T0
T1
T1+~5min

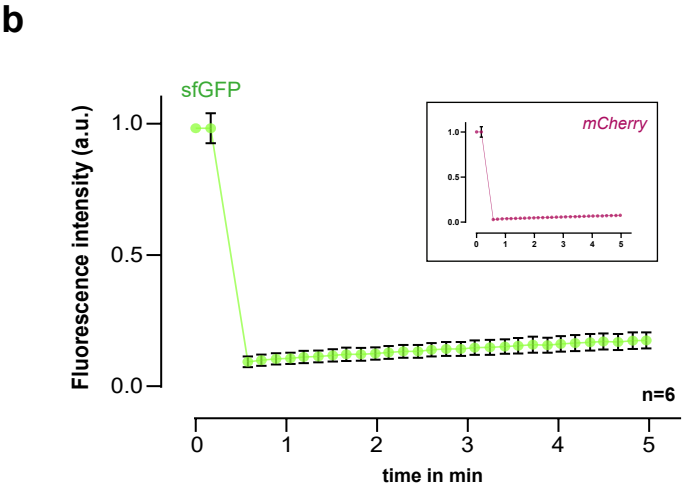
b
sfGFP
mCherry
Fluorescence intensity (a.u.)
1.0
0.5
0.0
n=6
0
1
2
3
4
5
time in min